BRNO UNIVERSITY OF TECHNOLOGY
VYSOKÉ UČENÍ TECHNICKÉ V BRNĚ

FACULTY OF MECHANICAL ENGINEERING
FAKULTA STROJNÍHO INŽENÝRSTVÍ

INSTITUTE OF MATERIALS SCIENCE AND ENGINEERING
ÚSTAV MATERIÁLOVÝCH VĚD A INŽENÝRSTVÍ

TERNARY SHAPE MEMORY ALLOYS POWDER FEEDSTOCK FABRICATION BY ADVANCED MECHANICAL ALLOYING

PŘÍPRAVA PRÁŠKOVÝCH PREKURZORŮ TERNÁRNÍCH SLITIN S TVAROVOU PAMĚTÍ MECHANICKÝM LEGOVÁNÍM PRÁŠKOVÝCH SMĚSÍ

BACHELOR'S THESIS
BAKALÁŘSKÁ PRÁCE

AUTHOR
AUTOR PRÁCE
Jan Regináč

SUPERVISOR
VEDOUCÍ PRÁCE
Ing. Jan Čížek, Ph.D.

BRNO 2016

Abstract
Powder metallurgy is used as an alternative method for producing Cu-based shape memory alloys. This method provided better results in the composition and grain size than conventional casting method. In the present work, mechanical alloying process is applied to convert the elemental powder mixtures of Cu-Al-Ni into pre-alloyed powders. The aim of this work was to find the optimal parameters to fabricate the most suitable powder feedstock intended for subsequent processing. SEM, EDX and X-ray Diffraction analysis have been used to characterize the effect of changing parameters on the obtained structure and possible formation of new phases. It was shown that high-energy milling is a suitable method for production of such pre-alloyed powders. Based on the results, it was found that a Cu-based solid solution was formed, independent on changing of parameters. The results further revealed that the high energy input in form of revolutions and long milling times, could cause a formation of amorphous phases.

Keywords
shape memory alloys, Cu-based shape memory alloys, powder metallurgy, mechanical alloying

REGINÁČ, J. *Ternary shape memory alloys powder feedstock fabrication by advanced mechanical alloying.* Brno: Brno University of Technology, Faculty of Mechanical Engineering, 2016. 47 p. Supervisor Ing. Jan Čížek, Ph.D.

I declare that I have personally compiled the thesis "Ternary shape memory alloys powder feedstock fabrication by advanced mechanical alloying", according to the instruction of my supervisor, Dr. Jan Čížek and with the use of the sources listed in bibliography.

Jan Reginác

I would like to sincerely express my thanks to my bachelor's thesis supervisor Ing. Jan Čížek, Ph.D. for his valuable advice, guidance and his willingness to help in every situation. I would also like to thank to Mgr. Jan Čupera for his patience and provided SEM micrographs. Further I would like to thank to Ing. Zdeněk Spotz, Ph.D. for provided X-ray diffraction results. Finally my thanks go to my family for supporting me during the studies.

Jan Reginář

Contents

1. Introduction

In recent years shape memory alloys (SMA, also called smart or intelligent materials) attracted much attention of designers, engineers and scientists. The ability to return to their memorized shape or size by a simple change of temperature makes them unique and useful for a wide range of applications.
From the existing SMA systems, Cu-based SMA are the most promising in a practical use because of their more competitive cost and easier fabrication process. The Cu-Al-Ni system has better thermal stability than other Cu-based SMA and was studied in the present work.
The most common preparation method of Cu-based SMA is a conventional casting method. However this method has some problems in controlling the grain size, which has a negative impact on mechanical properties of the alloys. Recently it has been reported that powder metallurgy (PM) with hot isostatic press (HIP) can be used as an alternative preparation method. Powder metallurgy processing is well-known for its capability of producing not only fine-grained materials but also near-netshape products on commercial scale. The most fascinating aspect of PM processing is that the desired microstructure and properties can be obtained by designing the process through a proper selection of starting powders and their subsequent processing [1]. Process of mechanical alloying provides prealloyed powders which can shorten sintering times.
In the present work, Fritsch high planetary mill was used to prepare powders feedstock from Cu-Al-Ni elemental powders mixture under different milling parameters. SEM, EDX and XRD analyses have been used to characterize the pre-alloyed powders. The purpose of this study is to find optimal parameters of mechanical alloying process in order to provide the most suitable powder feedstock intended for further processing.

2. Theoretical part

2.1. Shape memory alloys

2.1.1. History

The first solid phase transformation in shape memory alloys was discovered by Ölander in 1932. The Swedish physicist determined that the gold–cadmium alloys could be plastically deformed when cooled, and reverted to its original shape when heated [2]. The first shape memory effect (SME) was observed by Greninger and Mooradian in 1938 for copper–zinc alloys and copper–tin alloys. Later in 1949 Kurdjumov and Khandros reported the fundamental phenomenon of the shape memory effect governed by the thermoelastic behavior of the martensitic phase. The same observation was reported also by Chang and Read in 1951. Although similar effects in other alloys such as In-Tl and Cu-Al-Ni were also discovered in 1950s, the practical and industrial applications could not be realized due to their material high costs and unattractive properties.
In the early 1960s, Buehler and co-workers first explored the shape memory effect in an equiatomic NiTi alloy. This material, commonly referred to as "Nitinol", has been investigated extensively [3]. Nitinol alloys were cheaper to produce, easier and safer to handle, and had better mechanical properties compared to other existing SMA at that time. Since the 1980s, the commercial application of NiTi alloys has developed in many areas due to the greater demands for lighter and more compact actuators, especially in the biomedical sector [4].
In the 1990s SMA have found commercial application in broad range of industries including automotive, aerospace, robotics and biomedical.

2.1.2. Basic properties

Shape memory alloys are a unique class of shape memory materials with the ability to recover their shape when the temperature is increased (this transformation phenomenon is known as the shape memory effect). An increase in temperature can result in shape recovery even under high applied loads therefore resulting in high actuation energy densities. In addition, under specific conditions, they have high damping characteristic because of the ability to transform mechanical energy into thermal energy [5]. This irreversible energy transformation allows the material to resist shock and absorb vibrations [6]. Some of the mechanical properties (see Table 2.1) vary greatly over the temperature range between martensite and austenite phase, such as Young's modulus, electrical resistivity, thermal conductivity and thermal expansion coefficient. The austenite structure is relatively hard and has a much higher Young's modulus, whereas the martensite structure is softer and more malleable, i.e. can be readily deformed by application of an external force [4]. Although a large number of alloy systems exhibit SME (some of them are mentioned in Table 2.2), the most suitable systems that have achieved a level of commercial exploitation are the nickel-titanium alloys and copper-base alloys. Properties of these two systems are quite different as can be seen in Table 2.1 [6].

Table 2.1: Properties of commercially important shape memory alloys. A and M denote austenite and martensite respectively [6].

Property	**NiTi**	**CuAlNi**	**CuZnAl**
Melting temperature (°C)	1300	1000–1050	950–1020
Density (g/cm^{-3})	6.45	7.12	7.64
Thermal conductivity (W/g·°C)	18 (A)	30–43	120
	8.5 (M)		
Corrosion resistance	good	poor	poor
Young's modulus (GPa)	83 (A)	85 (A)	72 (A)
	28–41 (M)	80 (M)	70 (A)
Yield strength (MPa)	195–690 (A)	350 (A)	400 (A)
	70–140 (M)	80 (M)	130 (M)
Ultimate tensile strength (MPa)	895	500-800	600
Shape memory strain (%)	8.5 (max)	4	4

Table 2.2: Alloys exhibiting shape memory effect. Composition, transformation temperature range and approximate hysteresis of selected shape memory alloys [6].

Alloy	**Composition**	**Transformation range(°C)**	**Hysteresis(°C) (approximate)**
Ag-Cd	44–49 at%Cd	-190 to -50	15
Au-Cd	46.5–50 at%Cd	3 0 to 100	15
Cu-Al-Ni	14–14.5 wt%Al	-140 to 100	35
(3–4.5 wt%Ni)			
Cu-Sn	15 at%Sn	-120 to 30	-
Cu-Zn	38.5–41.5 wt%Zn	-180 to -10	10
Cu-Zn-X	few wt%X	-180 to 200	10
(X=Si, Sn, Al)			
In-Ti	18–23 at%Ti	60 to 100	4
Ni-Al	36–38 at%Al	-180 to 100	10
Ni-Ti	49–51 at%Ni	-50 to 110	30
Fe-Pt	25 at%Pt	-130	4
Mn-Cu	5–35 at%Mn	-250 to 180	25
Fe-Mn-Si	32 wt%Mn, 6 wt%Si	-200 to 150	100

2.1.3. The martensitic transformation and shape memory effect

The key characteristic of all SMA is the occurrence of martensitic phase transformation between the austenitic phase and the different variants of the low temperature, low symmetry martensitic phase (i.e. twinned martensite, detwinned martensite) [3]. The martensitic transformation is a shear dominant diffusionless solid state phase transformation. Martensitic structure is stable at lower temperatures and the austenite structure is stable at high temperatures.

When an SMA is heated, the martensitic transformation to austenite phase begins. The austenite start temperature (A_s) is the temperature where this transformation starts and the austenite finish temperature (A_f) is the temperature where this transformation is complete. Once a SMA is heated beyond A_s it begins to contract and transform into the austenite structure, i.e. to return into its original form. During the cooling process, the

transformation starts to revert to the martensite at martensite start temperature (M_s) and is complete when it reaches the martensite finish temperature (M_f) (see Fig. 2.1). The highest temperature at which martensite can no longer be stress induced is called M_d, and above this temperature the SMA is permanently deformed like any ordinary metallic material. These shape change effects, which are known as the SME and pseudoelasticity, can be categorized into three shape memory characteristics as follows:

1. One-way shape memory effect (OWSME): The one-way SMA (OWSMA) retains a deformed state after the removal of an external force, and then recovers to its original shape upon heating.

2. Two-way shape memory effect (TWSME) or reversible SME: In addition to the one-way effect, a two-way SMA (TWSMA) can remember its shape at both high and low temperatures.

3. Pseudoelasticity (PE): The SMA reverts to its original shape after applying mechanical loading at temperatures between A_f and M_d, without the need for any thermal activation [4].

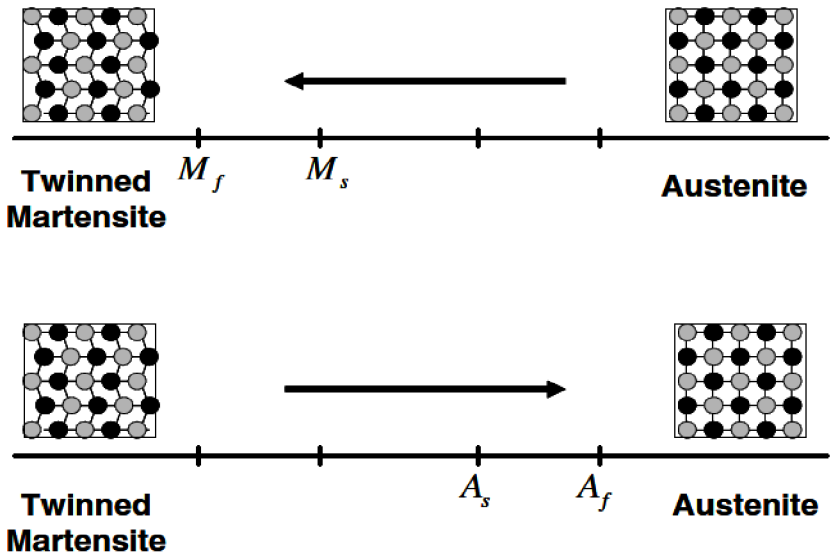

Figure 2.1: Temperature-induced phase transformation of an SMA without mechanical loading [5].

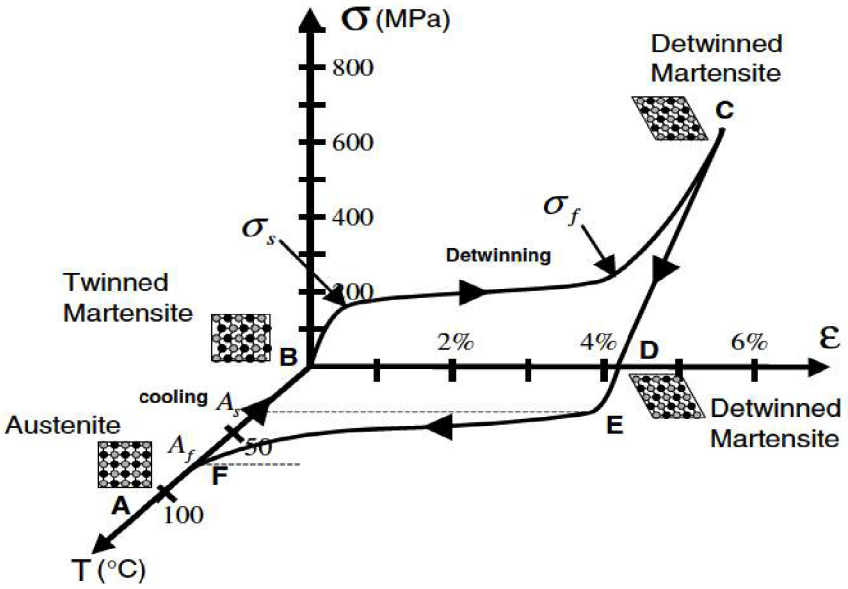

Figure 2.2: Stress-strain-temperature data exhibiting the shape memory effect for a typical NiTi SMA [5].

2.1.4. Processing of shape memory alloys

SMA can be prepared as any other metallic alloys, solidified from the liquid state at different cooling rates (conventional casting and fast quenching), by pressing and sintering powders, or by thin film physical or chemical vapour deposition. Due to their structural characterisitics, including the possible formation of thermally induced thermal martensitic transformations, special attention has to be paid to the control of the process. The main preparation methods are [7]:

- Melting and casting of ingots
- Thermo-mechanical processing
- Single crystals growth
- Thin films
- Powder metallurgy
- Rapid solidification

2.1.5. Shape memory alloys advantages and challenges

Nowadays SMA are slowly replacing common materials in applications, where the SME can be used, because of their extraordinary abilities and unique characteristics. For instance, the NiTi SMA display one of the highest work density at 10 J·cm^{-3}, which is the factor of 25 times greater than the density of electric motors and it is able to lift 100 times its own weight. In addition, the NiTi is also bio-compatible and exhibits high wear resistance [4]. Cu-based SMA have the advantages of low material cost and good workability in processing, and some of them even have the rubber-like behavior after aging in a martensitic state [8].

The challenges in designing SMA applications are to overcome their limitations, which include a relatively small usable strain, low actuation frequency and low energy efficiency. The major obstacle is the low actuation frequency and narrow bandwidth of SMA materials, which have a relatively high heat capacity and density, and as a result they experience difficulty in transferring the heat rapidly into and more importantly out of the active element [4].

2.1.6. Applications of shape memory alloys

Since SMA have unique properties which ordinary metals do not have, they have a high potential for many applications. The unique behavior of SMA have spawn new innovative applications in the aerospace, automotive, automation and control, appliance, biomedicine, robotics, energy, chemical processing, heating and ventilation, safety and security, and electronics industries.

- **Automotive applications:**
  In modern vehicles the number of sensors and actuators is increasing tremendously due to the demand for safer, more comfortable vehicles with better performance. The emerging driveby-wire technology offers a wide range of opportunities for SMA actuators as an alternative to electro-magnetic actuators in automotive applications. The existing and potential SMA applications for passenger vehicles are presented in Fig. 2.3. Most of the selected components are occasionally functioning as linear actuators (e.g. rear-view mirror folding, climate control flaps adjustment and lock/latch controls) and active thermal actuators (e.g. engine temperature control, carburetion and engine lubrication, and powertrain clutches). However, due to the SMA attractive morphing capability (active and adaptive structures), the applications are also expanding into other areas, such as aerodynamics and aesthetics applications [4].

- **Aerospace applications:**
  Since the success of the SMA coupling for hydraulic lines in the F-14 fighter jets in the 1970s, the unique properties of SMA have gathered greater interest in aerospace applications, which are subjected to high dynamic loads and geometric space constraints. A few examples of these applications are actuators [9], structural connectors, vibration dampers, sealers, release or deployment mechanisms, inflatable structures, manipulators, and the pathfinder application. In the 1990s, aerospace researchers focused on active and adaptive structures toward morphing capability and system-level optimization under various flight conditions (program 'smart wings') [10]. Boeing has developed an active serrated aerodynamic device with SMA actuators, which is also known as a variable geometry chevron (VGC). This device has proven to be very effective in reducing noise during take-off by maximizing the chevron deflection, and also increasing the cruise efficiency by minimizing the chevron deflection during the remainder of the flight [11].

- **Biomedical applications:**
  SMA have exhibited excellent behavior for biomedical applications such as high

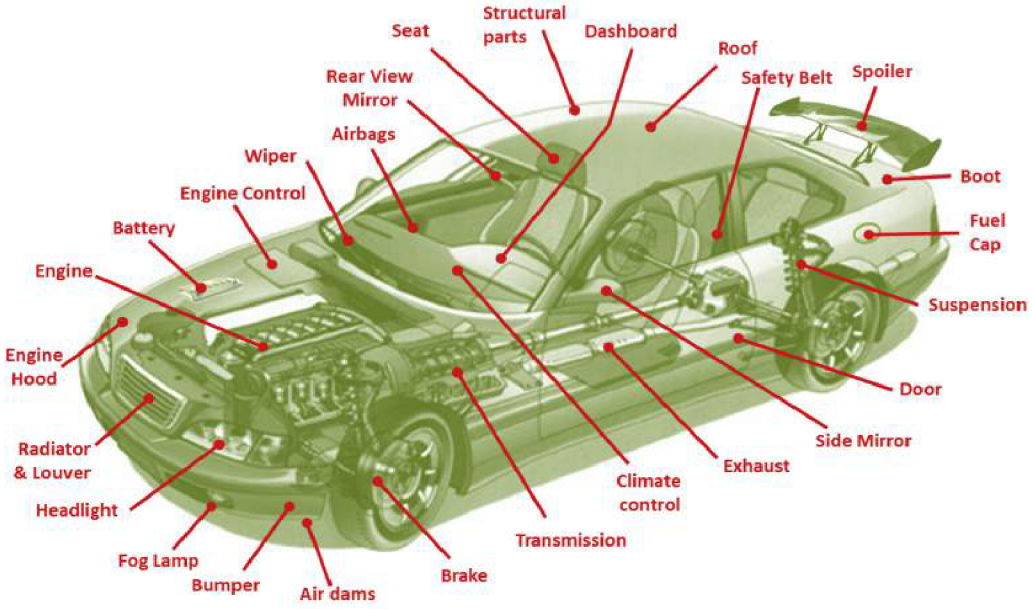

Figure 2.3: Existing and potential SMA applications in the automotive domain.

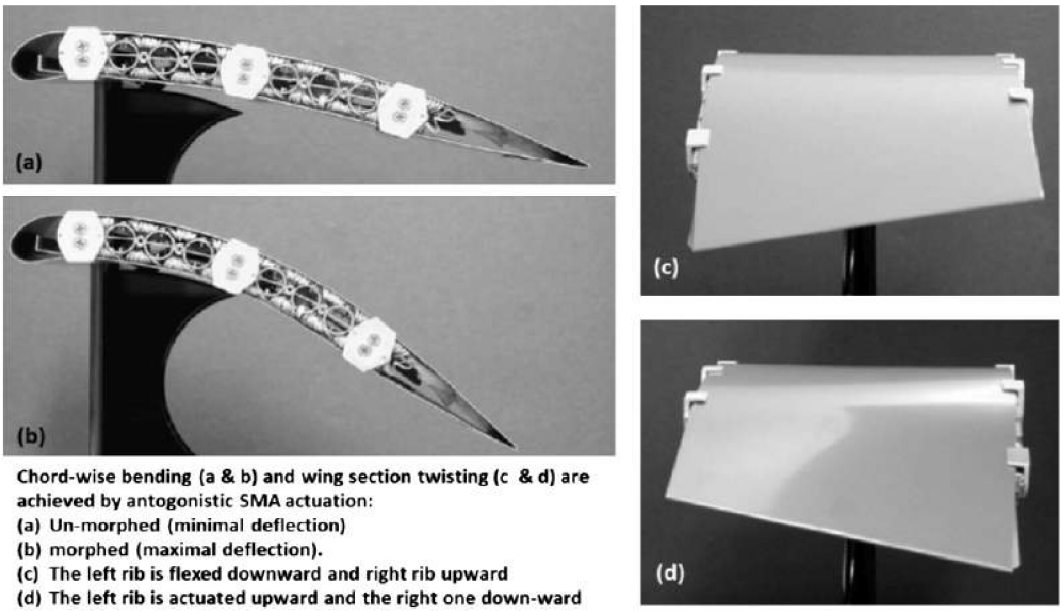

Figure 2.4: Wing morphing with antagonistic SMA actuators.

corrosion resistance, bio-compatible, non-magnetic, the unique physical properties, which replicate those of human tissues and bones, and can be manufactured to respond and change at the temperature of the human body. SMA are used in medical equipment and devices in many fields including orthopedics, neurology, cardiology and interventional radiology and other medical applications including: endodontics, stents, medical tweezers, sutures, anchors for attaching tendon to bone. The superelastic behavior of SMA, which fits the stress–strain behavior of human bone and tendons, makes it an excellent material to meet some of the challenges

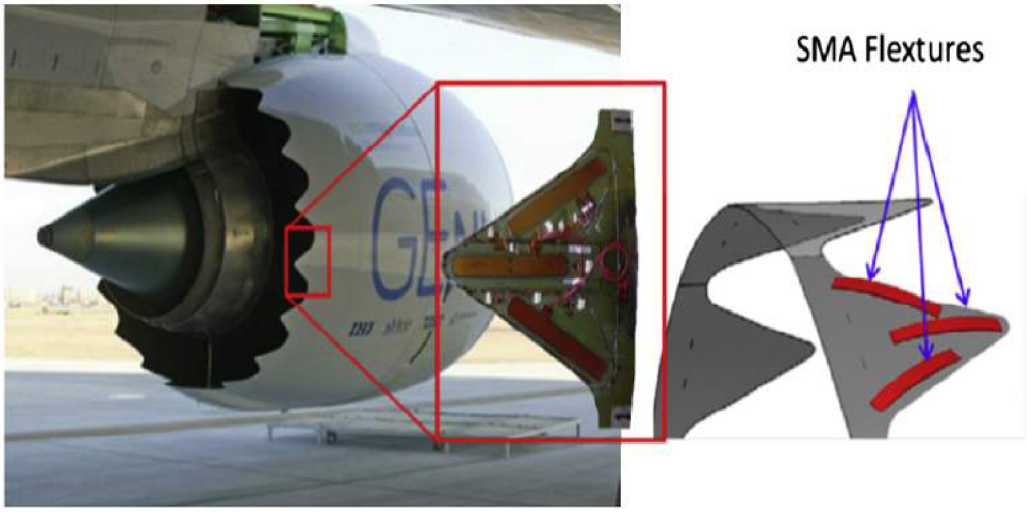

Figure 2.5: Boeing's variable geometry chevron (VSG).

presented by stenting operations [4].

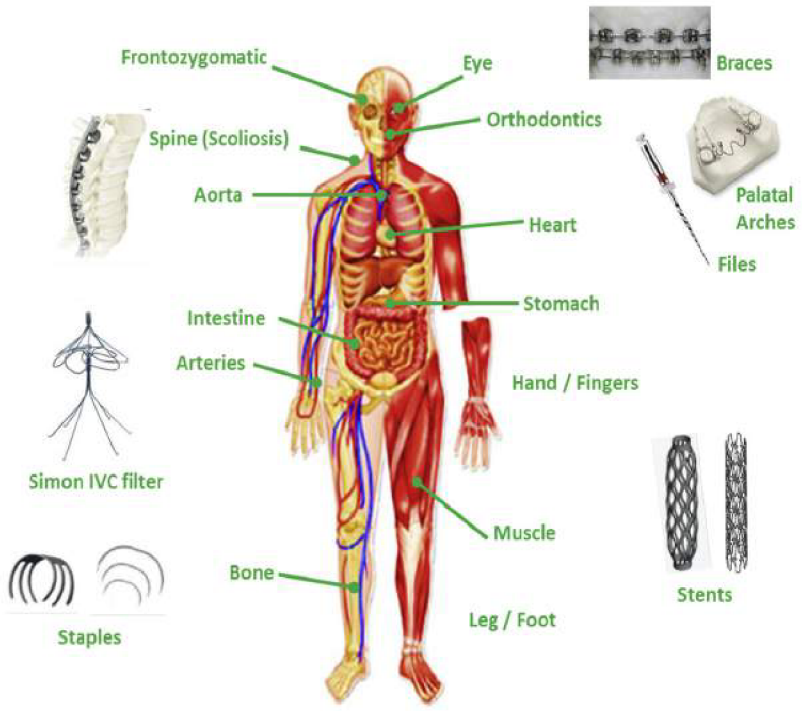

Figure 2.6: Existing and potential SMA applications in the biomedical domain.

2.1.7. Preparation methods of Cu-Al-Ni shape memory alloys

For the preparation of Cu-based SMA, the conventional casting method has difficulties in controlling the grain size. Coarse grains will weaken the mechanical properties of alloys [12]. Several attempts were made to improve the mechanical properties, especially ductility, of the conventionally cast Cu-Al-Ni SMA by grain refining via different techniques,

including thermo-mechanical treatment and additions of small amounts of quaternary elements, such as Zr, Ti, Co, and V [13]. Although these efforts resulted an improvement in the mechanical properties, such as strength and ductility, the mechanical properties were still unsatisfactory for most of the intended commercial applications.
It has been reported that mechanical alloying (MA) and powder metallurgy (PM) with hot isostatic press (HIP) can be used to fabricate Cu-based SMA [14]. MA produces pre-alloyed powders which can shorten the sintering time.

2.1.8. Applications of Cu-Al-Ni shape memory alloys

Cu-based SMA are commercially attractive alloys for practical applications owing to their low cost, together with a reasonable shape memory effect [15]. Among the Cu-based SMA, the Cu-Al-Ni alloys have increased thermal stability and offer possible use at higher temperatures. On the other hand, the practical applications of the Cu-Al-Ni alloys are restricted to those requiring very small shape changes due to their poor workability and susceptibility to brittle intergranular cracking [16]. An important goal for the Cu-Al-Ni alloys is to improve the mechanical properties by reducing the early mentioned limitations. Until now, research has shown that the mechanical properties of the Cu-Al-Ni alloys can be improved by adding alloying elements and by heat treatment [17].

Table 2.3: The most common specifications of the elemental powders.

	Cu-powder	**Al-powder**	**Ni-powder**
Composition of mixture (wt %)	82	14	4
	81.4	14.1	4.5
	13	4	83
	13.7	3.3	83.1
	11.9	3.8	84.3

2.2. Mechanical alloying

2.2.1. Introduction

Mechanical alloying (MA) is a solid-state powder processing technique involving repeated welding, fracturing, and rewelding of powder particles in a high-energy ball mill. The technique was developed by Benjamin around 1966 to develop an alloy combining oxide dispersion strengthening with γ' precipitation hardening in a nickel-based superalloy intended for gas turbine applications [18].
MA has now been shown to be capable of synthesizing a variety of equilibrium and non-equilibrium alloy phases starting from blended elemental or prealloyed powders. The synthesized non-equilibrium phases include supersaturated solid solutions, metastable crystalline and quasicrystalline phases, nanostructures, and amorphous alloys [19].

2.2.2. The process

The actual process of MA starts with mixing of the powders in the right proportion and loading the powder mix into the mill along with the grinding medium (generally steel or

ceramic balls). This mix is then milled for the desired length of time until a steady state is reached when the composition of every powder particle is the same as the proportion of the elements in the starting powder mix. The milled powder is then consolidated into a bulk shape and heat treated to obtain the desired microstructure and properties. Thus the important components of the MA process are the raw materials, the mill, and the process variables.
The raw materials used for MA are widely available commercially pure powders that have particle sizes in the range of 1–200 μm. The powder particle size is not very critical, except that it should be smaller than the grinding ball size. This is because the powder particle size decreases exponentially with time and reaches a small value of a few microns only after a few minutes of milling [19]. The raw powders fall into the broad categories of pure metals, master alloys[1], prealloyed powders, and refractory compounds.
Occasionally, metal powders are milled with a liquid medium and this is referred to as wet grinding, if no liquid is involved then it is referred to as dry grinding.
Different types of high-energy milling equipment are used to produce mechanically alloyed powders. They differ in their capacity, efficiency of milling and additional arrangements for cooling, heating, etc.
Mechanical alloying is a complex process and hence involves optimization of a number of variables to achieve the desired product phase and/or microstructure. Some of the important parameters that have an effect on the final constitution of the powder are:

- type of mill,
- milling container,
- milling speed,
- milling time,
- type, size, and size distribution of the grinding medium,
- ball-to-powder weight ratio,
- extent of filling the bowl,
- milling atmosphere,
- process control agent
- temperature of milling.

All these process variables are not completely independent. For example, the optimal milling time depends on the type of mill, size of the grinding medium, temperature of milling, ball-to-powder ratio, etc. [19].

[1]Master alloys are used to control the properties or crystal structure of various alloys.

2.2.3. Mechanism of alloying

During high-energy milling, the powder particles are repeatedly flattened, cold-welded, fractured and re-welded. Whenever two steel balls collide, some amount of powder is trapped in between them. Typically, around 1000 particles with an aggregate weight of about 0.2 mg are trapped during each collision (see Fig. 2.7) [19]. The force of the impact plastically deforms the powder particles leading to work hardening and fracture. The new surfaces created enable the particles to weld together and this leads to an increase in particle size [19]. Since in the early stages of milling, the particles are soft (if we are using either ductile-ductile or ductile-brittle material combination), their tendency to weld together and form large particles is high. A broad range of particle sizes develops, with some as large as three times bigger than the starting particles. The composite particles at this stage have a characteristic layered structure consisting of various combinations of the starting constituents. With continued deformation, the particles get work hardened and fracture by a fatigue failure mechanism and/or by the fragmentation of fragile flakes. Fragments generated by this mechanism may continue to reduce in size in the absence of strong agglomerating forces. At this stage, the tendency to fracture predominates over cold welding. Due to the continued impact of grinding balls, the structure of the particles is steadily refined, but the particle size continues to be the same. Consequently, the inter-layer spacing decreases and the number of layers in a particle increase.
However, it should be remembered that the efficiency of particle size reduction is very low, about 0.1% in a conventional ball mill. The efficiency may be somewhat higher in high-energy ball milling processes, but is still less than 1%. The remaining energy is lost mostly in the form of heat, but a small amount is also utilized in the elastic and plastic deformation of the powder particles [19].

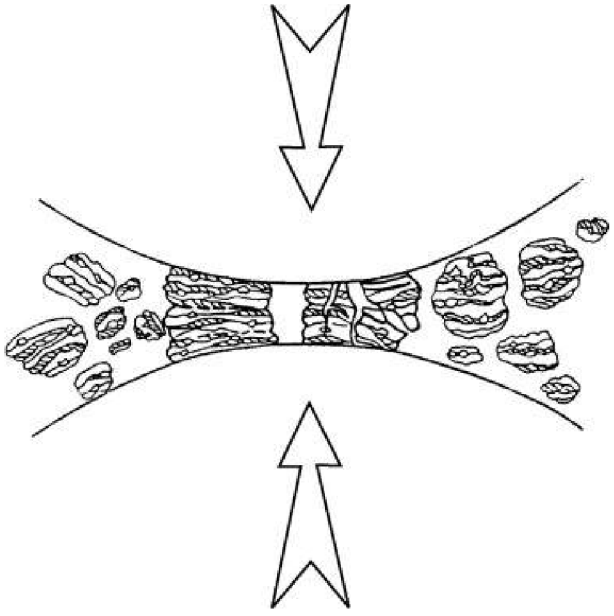

Figure 2.7: Ball powder collision of powder mixture during mechanical alloying.

During MA heavy deformation is introduced into the particles. This is manifested by the presence of a variety of crystal defects such as dislocations, vacancies, stacking faults, and increased number of grain boundaries. The presence of this defect structure enhances

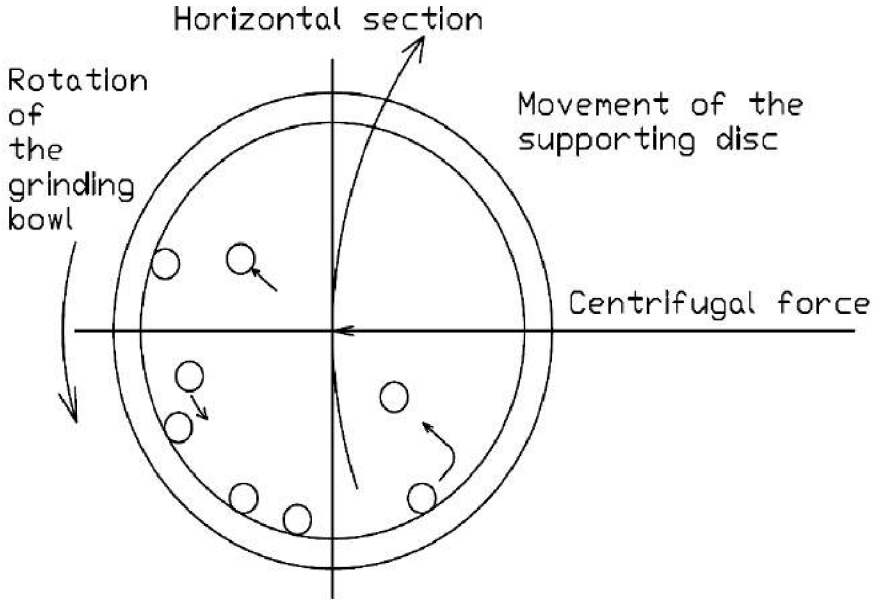

Figure 2.8: Balls movement during mechanical alloying.

the diffusivity of solute elements into the matrix. Further, the refined microstructural features decrease the diffusion distances. Additionally, the slight rise in temperature during milling further aids the diffusion behavior, and consequently, true alloying takes place amongst the constituent elements. While this alloying generally takes place nominally at room temperature, sometimes it may be necessary to anneal the mechanically alloyed powder at an elevated temperature for alloying to be achieved. This is particularly true when formation of intermetallics is desired [19, 20].

2.2.4. Advantages and disadvantages

The value of MA becomes apparent when attempts to make an alloy cannot be made by conventional routes. If the two metals form a solid solution, MA can be used to accomplish the same at lower temperatures. If the two metals are insoluble in solid state, i.e. immiscible solids (e.g. Cu-Fe) an extremely fine dispersion of one of the materials in the other can be achieved. MA represents cold alloying process, therefore it is suitable for hazardous operations. With proper precautions even volatile and inflammable materials can be handled safely [20]. In spite of the above mentioned advantages, the technique suffers from some problems.

- **Powder contamination:**
  The contamination of powders during MA is a major concern. The small size of the powder particles, availability of large surface area, and formation of new surfaces during milling all contribute to the contamination of the powder. In addition, the milling conditions (grinding medium, grinding bowl, time of milling, intensity of milling, etc.) and the atmosphere under which the powder is being milled also contribute to the contamination level. In many cases, especially when reactive metals like titanium and zirconium are being milled, the levels of contamination are high and unacceptable. Although several methods have been suggested to decrease/minimize the powder contamination level, the most effective ones seem to be (a) use of high-purity metals, (b) use of high-purity atmosphere, (c) use of balls

and container of the same material that is being milled, (d) self-coating of the balls with the milled material, and (e) shortest milling times [21].

- **Limited science content:**
  Although it is known that the technique works and so is useful, it is not very clear how and why the technique works. This is because MA is a complex stochastic process and the number of variables involved is too many. In spite of the complexity, some attempts have been made to model the process of MA and limited success has been achieved [21]. For example, it has been possible to establish a relation between the experimentally observed phase formation and some of the process variables. But, it has not been possible to predict the final chemical constitution (type and description of phases) for a given set of milling conditions [22].

2.2.5. Applications of mechanical alloying

MA has been used for developing alloys from immiscible liquids and solids, intermetallics and metastable phases. MA has emerged and developed in technology capable of providing unique PM materials with consistent properties for high performance applications over a wide range [20]. The major industrial applications of mechanically alloyed materials have been in the areas of thermal processing, glass processing, energy production, aerospace, and other industries [19].

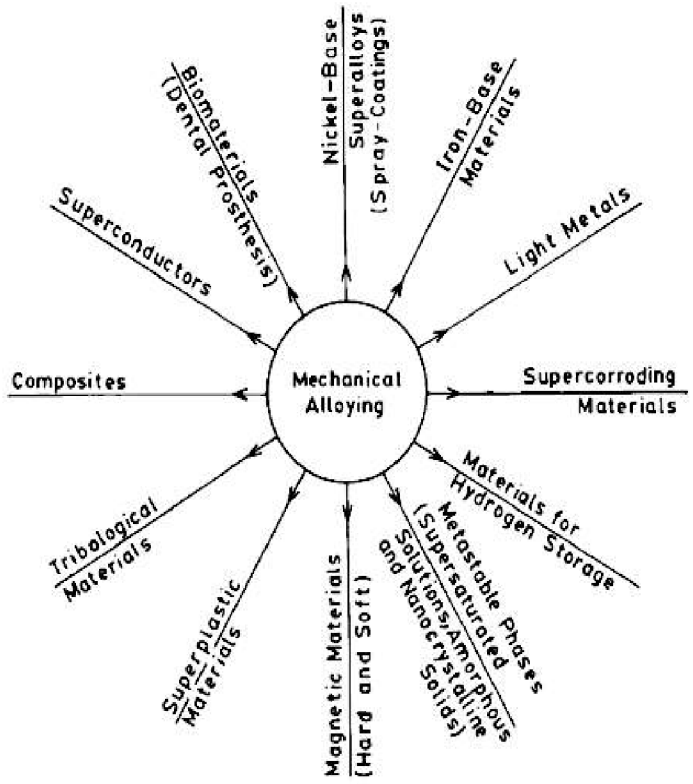

Figure 2.9: Application areas of mechanical alloying [20].

3. Experimental part

3.1. Materials

The powders in this study were prepared from elemental powders of copper, aluminum and nickel by mechanical alloying process. Composition of the mixture was 82% Cu, 14% Al and 4% Ni in wt%. All powders were supplied by GTV VerschleibSchutz GmbH Germany. Details of the microstructural characteristics and basic properties of the feedstock powders are discussed below. Selected physical and mechanical properties of the pure powders are provided in Tables 3.1; 3.2; 3.3.

3.1.1. Copper

Copper (symbol Cu, Cuprum in latin). It is a soft, malleable and ductile metal with very high thermal and electrical conductivity. A freshly exposed surface of pure copper has a reddish-orange color. It is used as a conductor of heat and electricity and as a constituent of various metal alloys [23].

Table 3.1: Physical and mechanical properties of copper [23].

Property	**Value**
Density (g/cm^{-3})	8.96
Young's modulus (GPa)	110
Yield strength (MPa)	210
Vickers hardness	38
Melting temperature (°C)	1084

Cu-powder with a chemical purity of 99.4% Cu (in wt%) was produced by water atomization method, which provides a typical irregular morphology of the particles (see Fig. 3.1). Particles with a size of 5–45 μm were suitable for the mechanical alloying process therefore further sieving was not necessary.

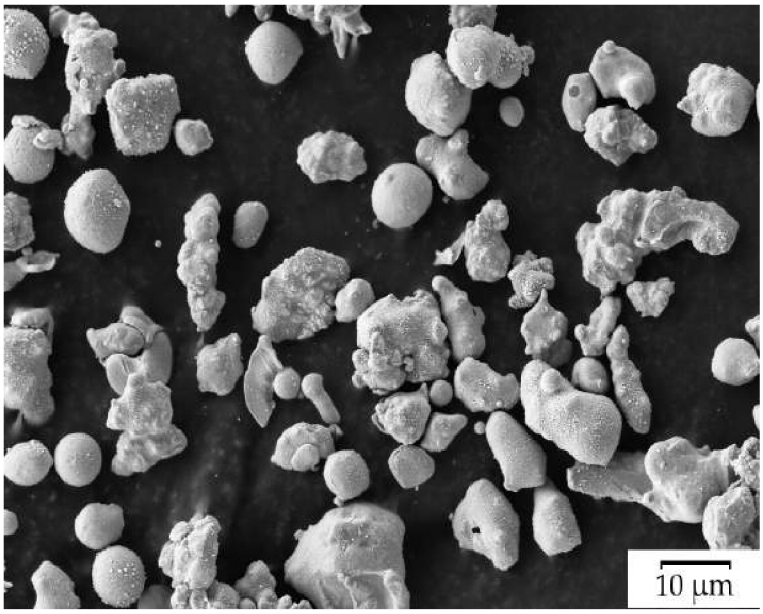

Figure 3.1: Morphology of the used Cu-powder particles.

3.1.2. Aluminum

Aluminum (symbol Al, Aluminium in latin). It is a silvery-white, soft, nonmagnetic, ductile metal. Aluminum is the third most abundant element in the Earth's crust (after oxygen and silicon) and it is the most abundant metal. Aluminum is remarkable for its low density and high corrosion resistance. Aluminum can be used in a wide range of applications e.g. electrotechnics and aerospace industry [23].

Table 3.2: Physical and mechanical properties of aluminum [23].

Property	**Value**
Density (g/cm^{-3})	2.7
Young's modulus (GPa)	62
Yield strength (MPa)	40–50
Vickers hardness	17
Melting temperature (°C)	660

The chemical composition of the used Al-powder consisted of 99,76% Al and 0,24% impurities (in wt%). The powder was produced by water atomization method and its particles size was around 20–53 μm. Figure 3.2 shows irregular morphology of the particles.

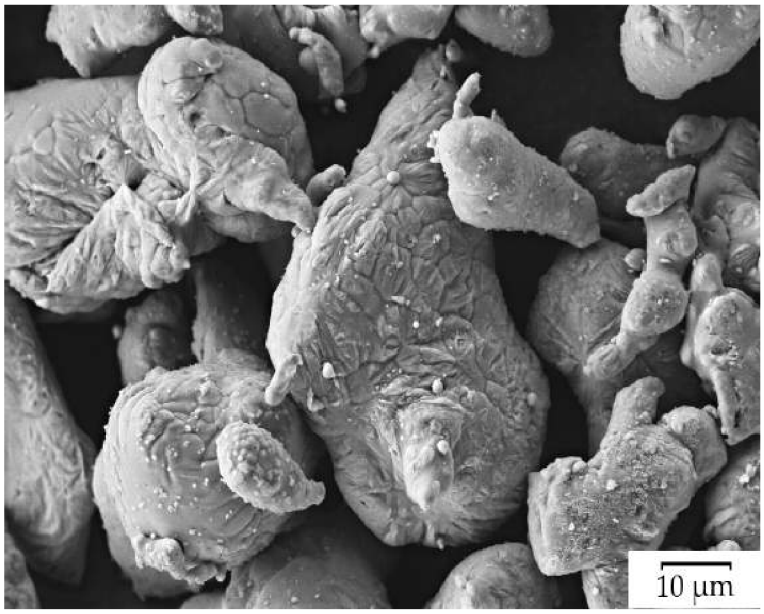

Figure 3.2: Morphology of the used Al-powder particles.

3.1.3. Nickel

Nickel (symbol Ni, Niccolum in latin). It is a silvery-white, ferromagnetic, hard and ductile metal. Nickel can be used as a compound of various alloys and also as a surface protection of other metals against corrosion. The practical use is somewhat limited due to its toxicity [23].

Table 3.3: Physical and mechanical properties of nickel [23].

Property	**Value**
Density (g/cm^{-3})	8.9
Young's modulus (GPa)	206
Yield strength (MPa)	140–195
Vickers hardness	65
Melting temperature (°C)	1455

Nickel's powder chemical analysis is following: 99,82% Ni and 0,18% impurities (in wt%). The powder was produced by gas atomization method, which provides almost ideal spherical shape of the particles (see Fig. 3.3). Particles size 15–53 μm was sufficient for the milling process, thus further processing was not needed.

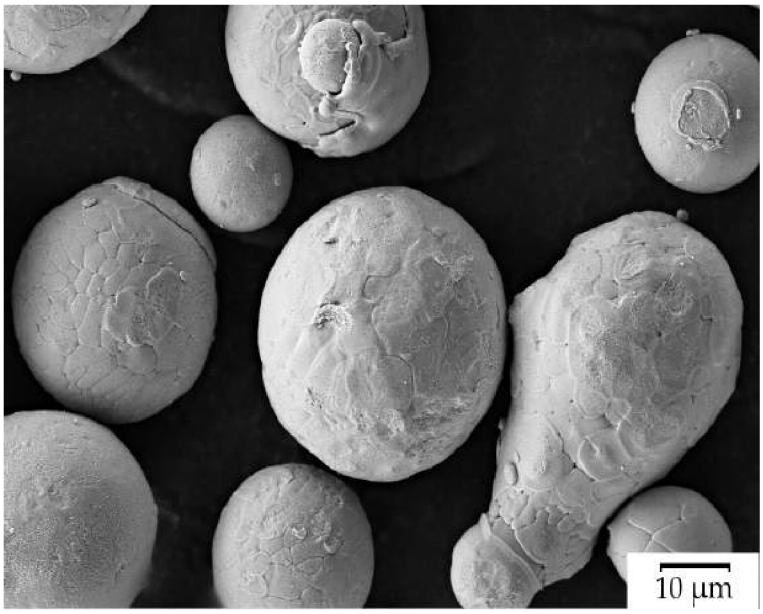

Figure 3.3: Morphology of the used Ni-powder particles.

3.2. Milling process

Cu-Al-Ni alloy powders were prepared by mechanical alloying process of elemental powders in a high energy planetary mill under different conditions. In the MA process, Fritsch Pulverisette 6 planetary mill with stainless steel jar was used. The jar was designed and manufactured at Brno University of Technology and allowed milling under protective nitrogen atmosphere. The jar was sealed by a gasket ring and tightened by five socket head screws in order to keep the atmosphere inside.
The process was realized under the pressure to prevent oxidation. After every 30 minutes of milling was the process paused for 30 minutes to allow jar cooling down and then further resumed for another 30 min.
True alloying process between the powder particles occurs when cold-welding and fracturing the particles are maintained in balance. Ethanol was added as a process control agent to control cold-welding between the particles and therefore inhibit extensive agglomeration.
The mechanical alloying process is highly dependent on variety of parameters. From all parameters named in section 2.2.2, the milling speed and milling time can be considered as the most influential, therefore they were chosen as variable representatives in this study. Other parameters were held as constant and their values are provided in Table 3.4.

Table 3.4: Annotation of constant parameters during the milling process.

Powder mixture weight	50 g
Balls material	Stainless steel
Balls diameter	10 mm
Ball to powder weight ratio (BPR)	5:1
Process control agent	Ethanol 100 ml
Milling atmosphere	Nitrogen

Maximum speed provided by a Fritsch Pulverisette 6 can be 650 RPM. The revolutions used in the experiment had to be considered carefully. Increasing the speed of rotation

will increase the speed with which the balls move and also influences, in which part of the bowl the balls will break away from the jar's inner wall. If a critical speed was exceeded, the balls would be pinned to the inner walls of the bowl and any impact force would not be achieved.
Maximum milling time that can be provided by a Fritsch Pulverisette 6 is 99 repetitions (50 hours). According to these limitations, various milling speeds and times (see Table 3.5) were selected. In total, 8 combinations of milling times and revolutions were used in this study. The range of the two parameters represented different intensities of milling, from high revolutions-short time (P01) to low revolution-long times (P07).

Table 3.5: Annotation of the mechanically alloyed powder samples.

Samples	**Milling time (h)**	**Milling speed (RPM)**
P01	10	400
P02	20	350
P03	20	300
P04	35	300
P05	50	300
P06	20	250
P07	50	250

3.3. Metallographic and chemical analysis

3.3.1. Preparation of the specimens for microscopy observation

After MA process it was necessary to separate the mixture from the steel balls first. The material with the balls could not be sieved, since the Ethanol process control agent caused the mixture to be wet. Thereby the mixture was spread on the paper to provide better drying. After drying process the balls were separated from the dried mixture by sieving. For observation of the prepared powders cross-sections, a small amount of the alloyed powder was mounted using a hot compression in ClaroFast and GreenFast resins. The mounting media was heated to a temperature of 180 °C for 8 minutes. Samples grinding and polishing was realized on a grinder from Struers company using abrasive papers and diamond suspensions from the same company. Papers with grain-size distribution 1000 and 1200 were used for grinding process. In order to get a finer results, the polishing was executed by using a magnetic platen and diamond suspensions with grain size 3 μm and 1 μm.

3.3.2. LM, SEM observation and EDX analysis

Using a light microscope Zeiss Axio Observer Z1, the samples could be observed under a variety of magnifications (10×, 20×, 50×, 100×). The light microscope revealed the morphology of examined samples. It was possible to observe a grain size distribution and their mutual cohesion.
Prior to SEM observations, carbon layers were deposited on the prepared samples in order to achieve better electrical conductivity. Zeiss Ultra Plus microscope using the secondary

electrons and back-scattered electrons, allowed the observation under different magnifications. With SEM technology it was possible to determine the morphology of powder particles with greater field of depth and higher magnifications than with the light microscopy.
Concerning the chemical analysis of the samples, the EDX analysis was performed. With an application of mapping, point and area analysis methods the exact chemical composition after alloying was provided. The SEM and EDX analysis provided results showing the impact of the changing parameters on the samples microstructure. From the obtained data, further combinations of the milling parameters to produce other alloyed powders were determined.

3.3.3. XRD analysis

X-ray powder diffractometer Rigaku SmartLab 3kW was applied to identify the phases in the starting feedstock powders as well as the alloyed powder mixtures. This system has θ/θ closed loop goniometer drive system, cross beam optics, which makes it easy to switch between Bragg-Brentano and Parallel Beam modes and enable various measurement. A few tenths of gram of the powders were put into sample holder. The X-rays were directed at the sample, and the diffracted rays were collected. As the result, characteristic X-ray spectra were obtained. With the help of X-ray patterns it was possible to observe if any prospective phase changes in the examined materials.

4. Results and discussions

4.1. Powders structure and morphology

As mentioned in chapter 3, SEM observations allowed to determine the effect of MA variable parameters on morphology and internal structure of the formed grains. It was possible to observe typical grain size and the cohesion between originated phases, as well as their mutual bonding and inter-mixing within the individual grains. The micrographs in Figs. 4.1 to 4.7 are presented at two different magnifications (50× and 200×) to provide more information on the internal structure of the particles cross-sections.

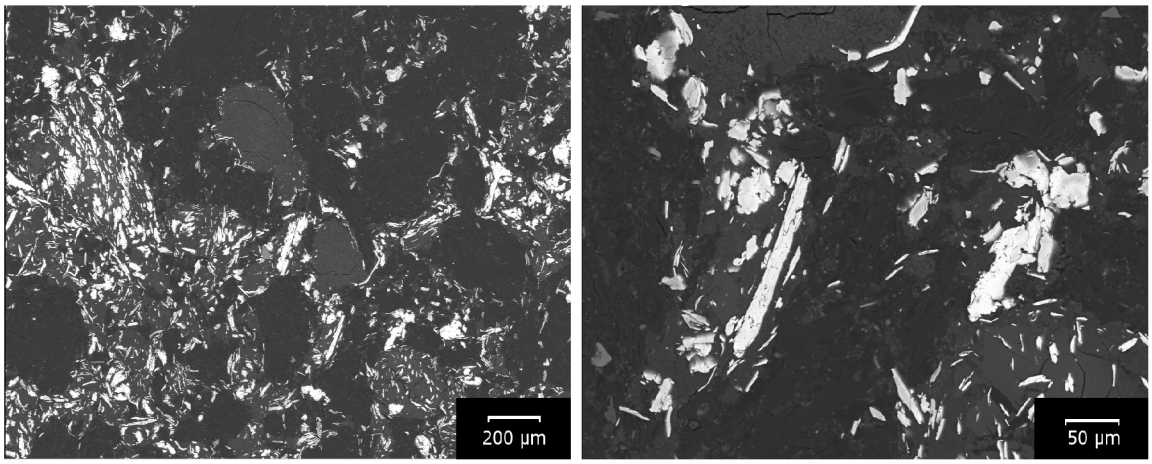

Figure 4.1: Sample P01 (400 RPM, 10 hr)

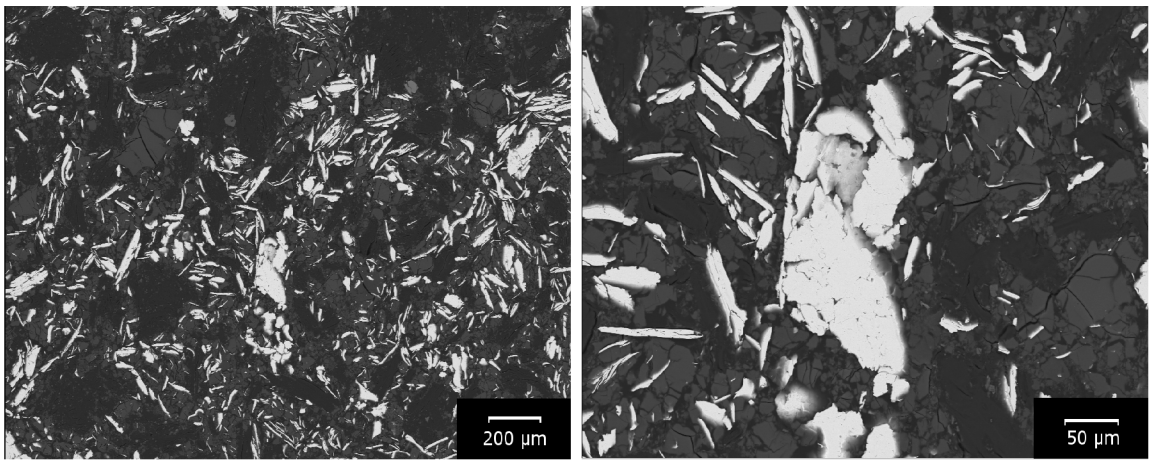

Figure 4.2: Sample P02 (350 RPM, 20 hr)

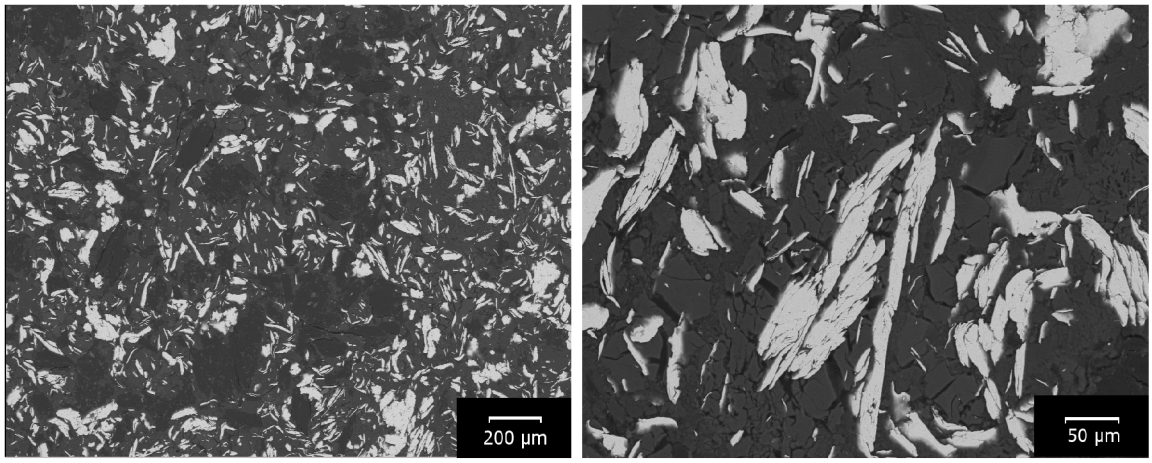

Figure 4.3: Sample P03 (300 RPM, 20 hr)

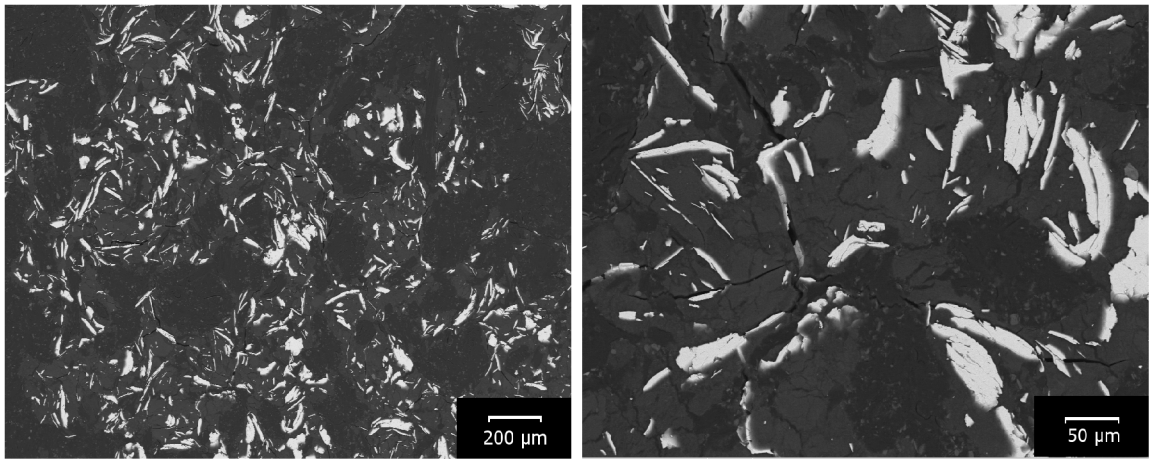

Figure 4.4: Sample P04 (300 RPM, 35 hr)

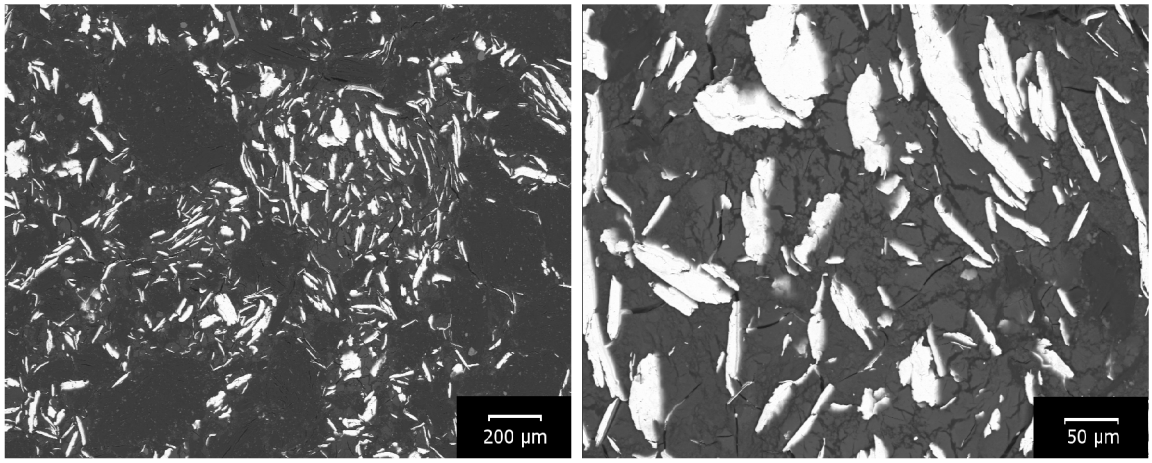

Figure 4.5: Sample P05 (300 RPM, 50 hr)

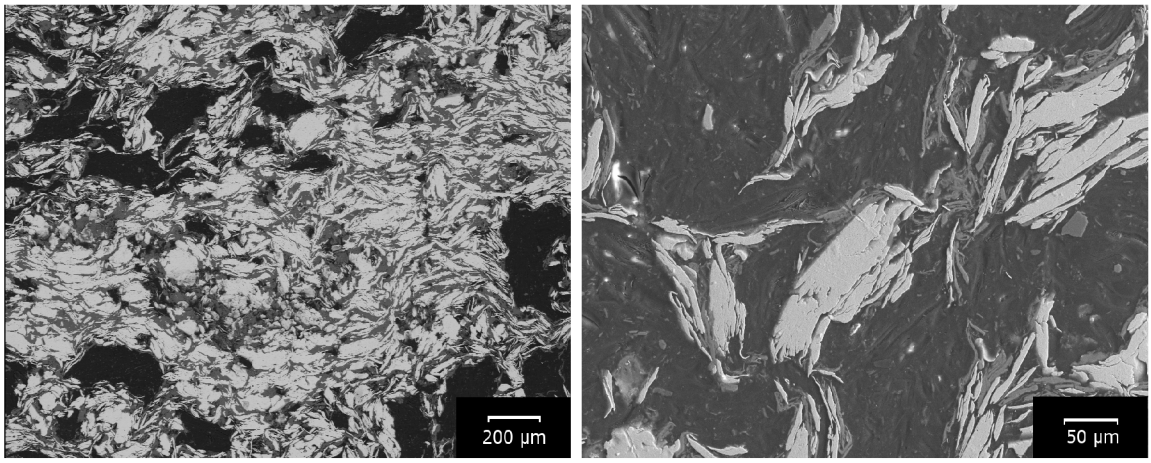

Figure 4.6: Sample P06 (250 RPM, 20 hr)

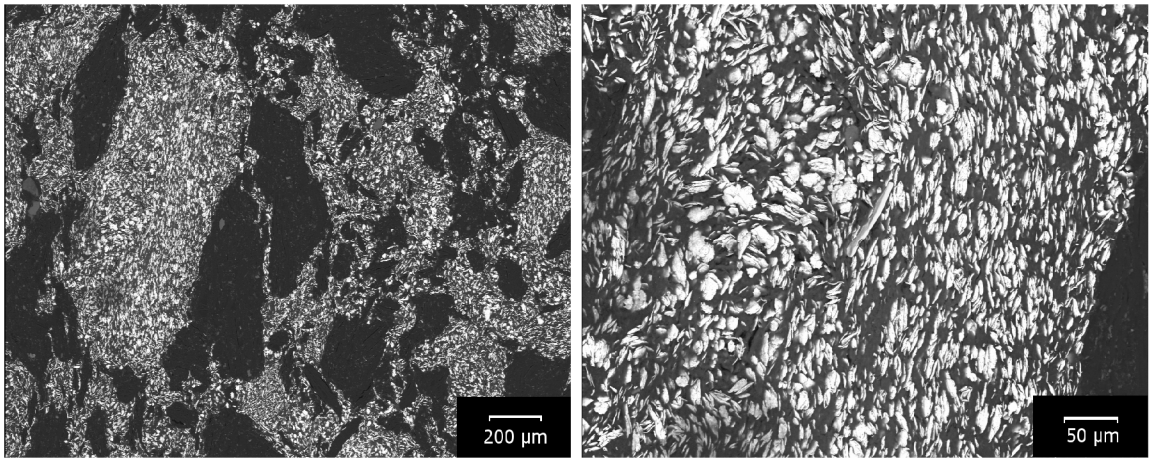

Figure 4.7: Sample P07 (250 RPM, 50 hr)

The images in Figs. 4.1 to 4.7 were obtained under back-scattered electron mode, allowing to differentiate materials of dissimilar chemical composition. The dark areas consist of Al particles embedded into the bright areas of Cu particles. Small content of Ni particles was observed in the form of individual grains, preferably attached to Cu particles. Due to similar contrast with Cu particles, the determination of Ni particles was substantially difficult, therefore high magnifications were required. Figure 4.1 shows morphology of the P01 sample. From the obtained results it can be concluded that high energy input in form of 400 RPM caused the formation of relatively coarse grains. Intensive cracking was observed mainly for the Al particles, probably a consequence of extensive cold-working process at such high milling intensities. Similar results were obtained by lowering revolutions to 350 RPM and extending time for 20 hours. In this case the particles were still very dispersed and brittle as can be seen in Fig 4.2. Concerning the samples shown in Fig 4.3, 4.4, 4.5 the revolutions were held the same, i.e 300 RPM. The effect of extending the milling times caused change in the intensity of cracking of the Al grains. As opposed to milling at higher revolutions, the Cu grains did not exhibit any substantial cracking at 300 RPM, i.e. the intensity of the impacting milling balls did not result into depletion of the plasticity even after 50 hours of milling. Fabrication of such samples aided in determination of the correct parameters as it suggested further lowering of the mill revolutions for the next samples.

Further lowering revolutions to 250 RPM lead to a substantial change in the morphology of the produced grains as flattened lamellae were now observed in Figs. 4.6 and 4.7. However after 20 hours at 250 RPM, the Cu particles were not joined seamlessly, which is probably a consequence of the low energy input into the material. With the extending of milling time to 50 hours, the lamellar structure was more plastically deformed and became slightly more brittle. Brittle particles can be easily fractured into smaller pieces. Therefore the structure observed in sample P07 became more refined than structure obtained after 20 hours of milling, as it is shown in Fig 4.7. In general, it could be concluded that the global morphology of the Cu-Al-Ni particles after the milling process is mainly influenced by the used revolutions parameter, which can change also influence the extent of cracking and the level of mutual grains coalescence. Secondary to that is the milling time where, within the used span of 10–50 hours changes were also recorded. From the point of view of future compaction of the powder for SMA applications, the optimum powder mixtures were obtained at low RPM (250) and extended milling times (50 hours).

4.2. Chemical composition

On the basis of provided EDX results it was possible to identify the occurrence of individual elements within the alloyed powders. The obtained results revealed that mechanical alloying process seems to be suitable for joining copper and nickel together and caused the formation of solid solution of these two elements. In Fig 4.8, the solid solution of Cu and Ni is marked by arrow 1. Such result suggested that, apart from the observed individual Ni grains, some Ni content in the powder was incorporated into the Cu particles, too. The dark areas marked by arrow number 2 consist of aluminum and certain amount of oxygen. Its content was measured to vary from 5–32% in the samples (Table 4.1). However, it needs to be understand that the EDX method is very insensitive to determination of content of light elements such as oxygen or carbon and therefore the EDX maps provide qualitative distribution of oxygen only. Comparing the maps of individual elements (Fig. 4.8), it could be concluded that the oxidized material was Al only and the Cu-Ni grains were not affected. It is not clear at the moment whether the oxygen content was present in the original Al feedstock already or whether it was formed within the milling process.

Table 4.1: Annotation of the chemical composition after mechanical alloying process.

Samples	**Cu (in wt %)**	**Al (in wt %)**	**Ni (in wt %)**	**O (in wt %)**
P01	39 %	30 %	2 %	29 %
P02	41 %	30 %	2 %	27 %
P03	38 %	31 %	2 %	29 %
P04	34 %	32 %	2 %	32 %
P05	46 %	33 %	3 %	18 %
P06	48 %	44 %	3 %	5 %
P07	52 %	29 %	2 %	17 %

As seen from Table 4.1, the milling parameters almost did not affect the content of nickel in the samples. The composition Al was measured to fluctuate around 30 %. The observed quantitites of Cu, Al and Ni content differ substantially from the original feedstock composition of Cu-14Al-4Ni ratio. This is most likely caused by the fact that their

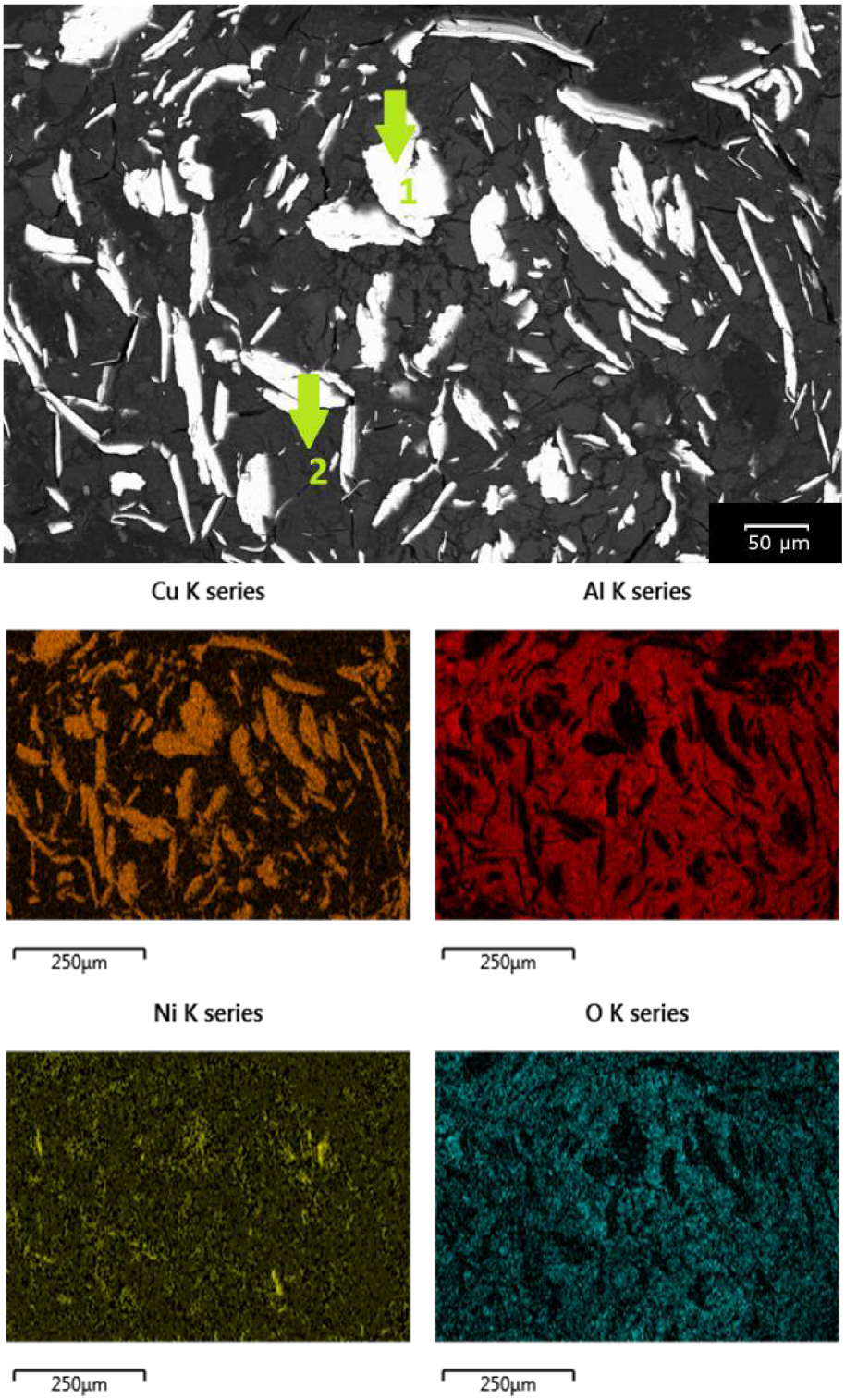

Figure 4.8: EDX mapping of typical alloyed powder microstructure. Arrows indicate two phases retained in the milling process (1-Cu+Ni, 2-Al) and the elemental maps show distribution of the three main elements (Cu, Al, Ni) as well as the inevitable oxygen content.

individual contents were determined from 2D cross-section of the powders. Given their respective morphologies (plate-like milled Cu and Ni particles in equiaxed Al matrix),

the numerical determination of Cu, Ni is highly underrated as the cross-sections do not represent the total volume of Cu, Ni and vice versa for the Al content.
While the formation of the copper and nickel solid solution was observed for each combination of variable parameters, the third compound aluminum was not embedded in. From the EDX layered maps in Fig 4.8 and figures attached in Appendix A, a certain correlation between copper-nickel solid solution and aluminum can be observed. Aluminum together with oxygen cannot be found in grains where a high density of copper and nickel particles appears. It could be concluded that aluminum did not diffuse into copper-nickel grains in spite of increased temperatures caused by the milling process.

4.3. X-ray Diffraction analysis

XRD pattern of the initial mixed-only powder feedstock is shown in Fig. 4.9. This pattern was regarded as a reference condition where the peaks of starting elements appeared. During the milling, the phase composition of the powders changed significantly, a consequence of the extensive deformation process and generated heat. The Fig. 4.10 shows the phase evolution during the MA alloying processes performed under different milling conditions. The peaks of aluminum element occurred in the samples when the revolutions

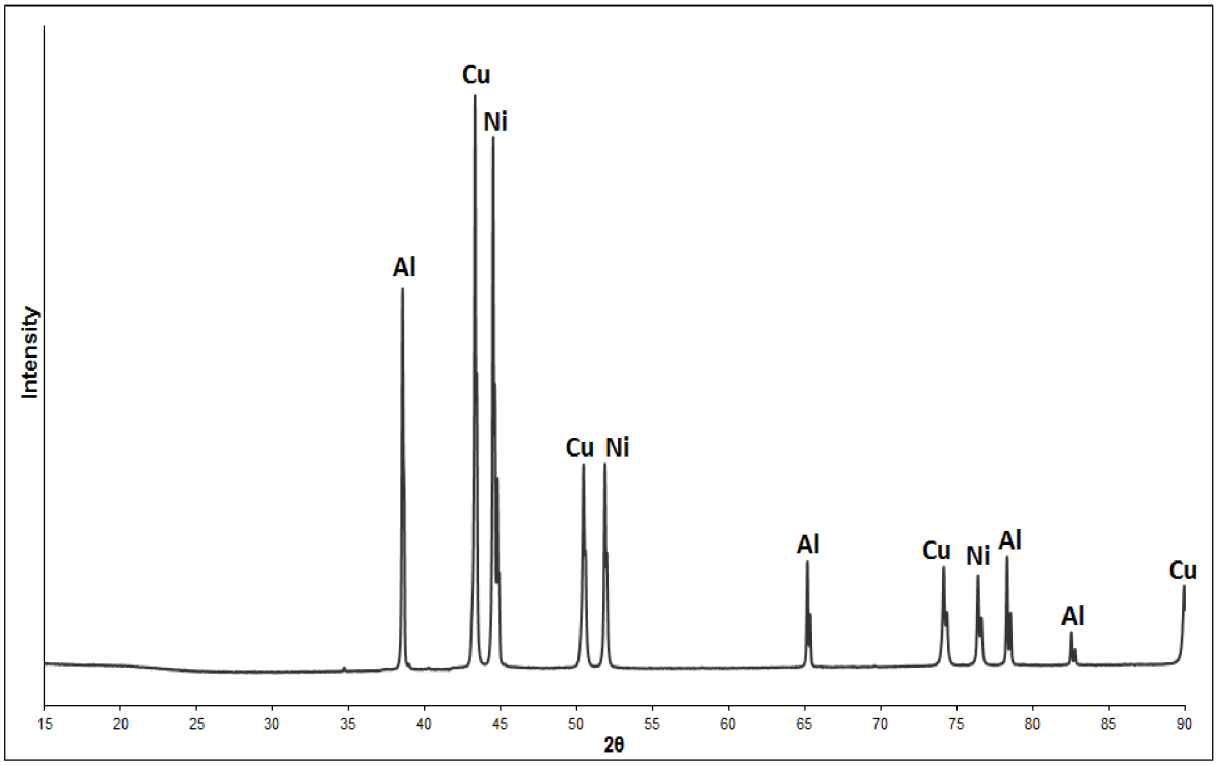

Figure 4.9: X-ray Diffraction pattern of starting elements.

were set to 250 RPM. The content of aluminum phase was measured to a value of 20 % (Table 4.2) after 20 hours of milling and its peaks were observed clearly. After 50 hours of milling the Al peaks became almost indistinguishable. During the further increase to higher revolutions, the Al peaks vanished completely.

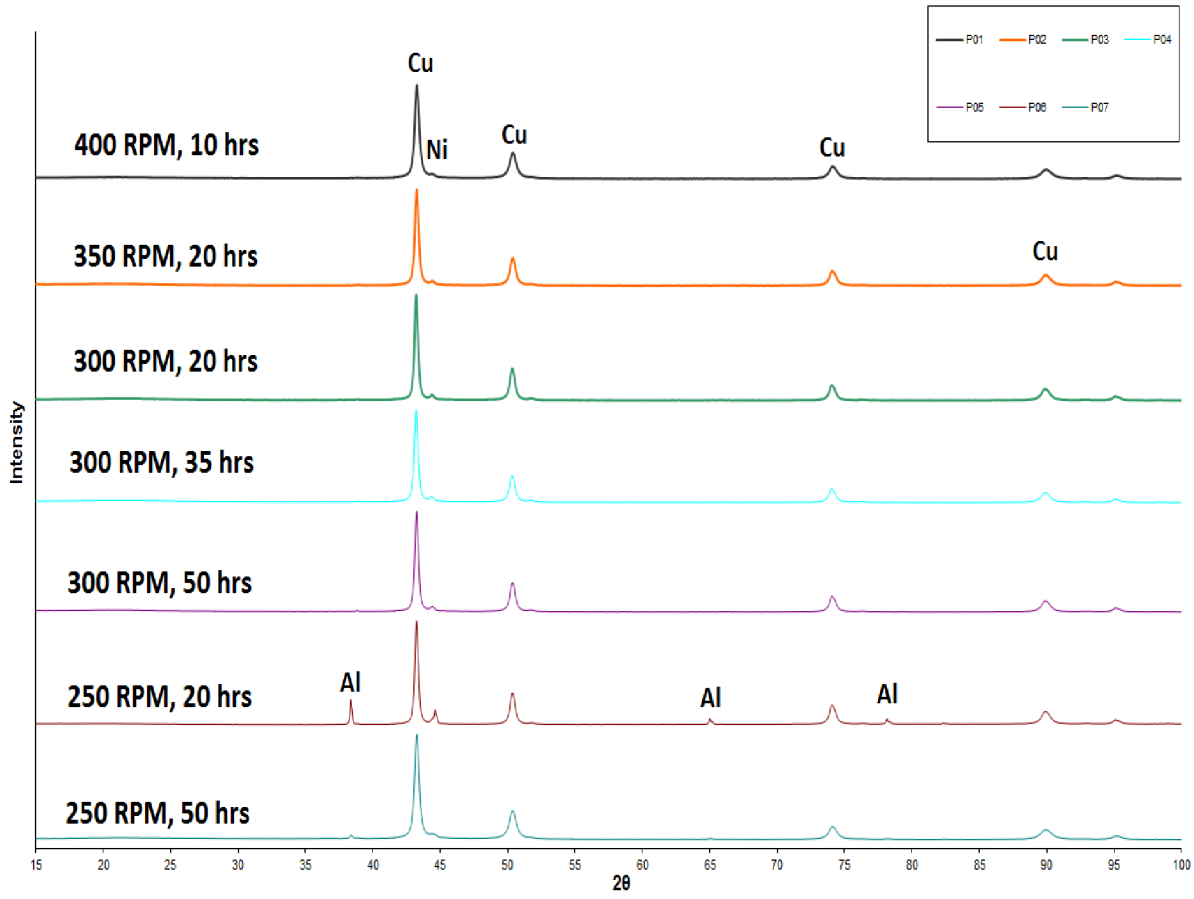

Figure 4.10: Phase composition of the powders milled at different conditions. Note the diminishing Al peaks toward more intensive milling.

Table 4.2: Phase content of the samples and main peaks width (FWHM).

Samples	Phase content(%)			Peak width(°)		
	Cu	**Al**	**Ni**	**Cu**	**Al**	**Ni**
Cu	100	0	0	0.014	0	0
Al	0	100	0	0	0.010	0
Ni	0	0	100	0	0	0.010
P01	94.6	0	5.4	0.144	0	0.200
P02	93.6	0	6.4	0.090	0	0.180
P03	93.7	0	6.3	0.078	0	0.084
P04	92.8	0	7.2	0.099	0	0.122
P05	93.2	0	6.8	0.086	0	0.123
P06	74.5	20	5.5	0.077	0.015	0.197
P07	91.1	4	4.9	0.158	0.039	0.200

The patterns for samples P01–P05 behave almost identical. Slight differences can be seen in the peak width, where almost all peaks became 10× wider than peaks obtained before alloying (see Table 4.2). It can be concluded that the higher energy input in form of revolutions or long milling times, triggered intensive reduction of the size of individual crystallites.

In accordance of above provided EDX results, the XRD technology confirmed the occur-

rence of the single copper and single nickel phase in all examined samples (Table 4.2), whereas the single aluminum phase appeared in samples P06 and P07 only. The lattice parameters of Cu-Al-Ni phases were found to be close to parameters before alloying.
The chemical composition of alloyed powders feedstock provided by EDX analysis (see Table 4.1) showed the content of aluminum in every sample. Also, the individual Al particles were observed in SEM imaging. However, the phase XRD analysis of the higher-intensity milled powders (P01–P05) did not detect any traceable Al content whatsoever. According to provided results and literature research, the formation of amorphous phases could be considered as an explanation. Suryanarayana [19] evidences a number of reports on the formation of amorphous phases by MA in several binary and ternary (and a few higher order) alloy systems. The amorphous phase formation is known to be critically dependent on the milling conditions, e.g mill type, milling jar, grinding medium, ball to powder ratio, and other parameters. It has been reported that increased milling energy (achieved by increased speed of rotation etc.) is normally expected to introduce more strain and increase the defect concentration in the powder and thus lead to easier amorphization [19]. This fact confirms the provided results, when the speed of rotation is over 300 RPM the aluminum phase is transformed into amorphous phase, thus the XRD technology was not able to identify Al peaks. Under smaller revolutions (250 RPM), the Al content secondly depended on the milling time. With the extending of milling time the content of Al reduced, again in accordance with e.g. [12].
No intermetallic phases formation was detected in the fabricated powders. This fact is somewhat surprising considering the nature of the milling and the substantial amount of heat generated during the process. As such, further heat treatment of the compact might be required to introduce intermetallic phases formation.

5. Conclusions

In this study, mechanically alloyed Cu-14Al-4Ni samples were milled under different milling conditions. Their resulting morphology, size and cross-section features were evaluated subsequently, as well as their chemical and phase composition. In the study, high quality alloyed powder was obtained within the optimization phase. From the results, the following conclusions can be drawn:

- The global morphology of the Cu-Al-Ni particles after the milling process is mainly influenced by the used mill revolutions parameter. This parameter further influences the extent of cracking and the level of mutual grains coalescence.
- The optimum powder mixture for further compaction processes was obtained at low revolutions (250) and extended milling time (50 hours).
- Aluminum did not diffuse into copper-nickel grains in spite of increased temperatures caused by milling process.
- Aluminum content is amorphized within the milling process. The process is time dependent and the amorphization times are substantially reduced at the increased revolutions (exceeding 300RPM).
- No intermetallic phases were formed during the milling. Therefore further heat treatment of the compact might be required to introduce intermetallic phases formation.

Bibliography

[1] VAJPAI, S. K., DUBE, R. K. and SANGAL, S. Application of rapid solidification powder metallurgy processing to prepare Cu–Al–Ni high temperature shape memory alloy strips with high strength and high ductility. *Materials Science and Engineering*, 2013, Vol. 570, p. 32-42. ISSN 09215093.

[2] ÖLANDER, A. An electochemical investigation of solid cadmium-gold alloys. *Journal of the American Chemical Society*, 1932, Vol. 54, no. 10, p. 3819-3833. ISSN 00027863.

[3] PATOOR, E., et al. Shape memory alloys, Part I: General properties and modeling of single crystals. *Mechanics of materials*, 2006, Vol. 38, no. 5, p. 391-429. ISSN 0167-6636.

[4] JANI, J. M., et al. A review of shape memory alloy research, applications and opportunities. *Materials and Design*, 2014, Vol. 56, p. 1078-1113. ISSN 0261-3069.

[5] LAGOUDAS, D. C. Shape memory alloys: modeling and engineering applications. *Springer Science and Business Media*, 2008, p. 1-51. ISBN 978-0-387-47685-8.

[6] KRISHNAN, R. V., BHAUMIK, S. K. Shape memory alloys: properties and engineering applications. In: Smart Materials, Structures, and Systems.*International Society for Optics and Photonics*, 2003, p. 879-890. ISSN 0277786X.

[7] OCHIN, P. Processing and synthesis of shape memory alloys. *Archives of Metallurgy and Materials*, 2004, Vol. 49, no. 4, p. 753-763. ISSN 1733-3490.

[8] HUANG, W. M., et al. Shape memory materials. *Materials Today*, 2010, Vol. 13, no. 7, p. 54-61. ISSN 1369-7021.

[9] HARTL, D. J., LAGOUDAS, D. C. Aerospace applications of shape memory alloys. Proceedings of the Institution of Mechanical Engineers, Part G. *Journal of Aerospace Engineering*, 2007, Vol. 221, no. 4, p. 535-552. ISSN 09544100.

[10] KUDVA, J. N. Overview of the DARPA smart wing project. *Journal of Intelligent Material Systems and Structures*, 2004, Vol. 15, no. 4,p. 261-267. ISSN 1045389x.

[11] OEHLER, S. D., et al. Design optimization and uncertainty analysis of SMA morphing structures. *Smart Materials and Structures*, 2012, Vol. 21, no. 9, p. 094016.

[12] TANG, S. M., CHUNG, C. Y., LIU, W. G. Preparation of Cu Al Ni-based shape memory alloys by mechanical alloying and powder metallurgy method. *Journal of materials processing technology*, 1997, Vol. 63 no. 1, p. 307-312. ISSN 09240136.

[13] GAO, Y., ZHU, M., LAI, J. K. L. Microstructure characterization and effect of thermal cycling and ageing on vanadium-doped Cu–Al–Ni–Mn high-temperature shape memory alloy. *Journal of materials science*, 1998, Vol. 33, no. 14, p. 3579-3584. ISSN 1573-4803.

[14] KIM, Y. D., WAYMAN, C. M. Shape memory effect in powder metallurgy Ni-Al alloys.*Scripta Metallurgica et Materialia*, 1990, Vol. 24, no. 2, p. 245-250. ISSN 0956716x.

[15] SARI, U., KIRINDI, T. Effects of deformation on microstructure and mechanical properties of a Cu–Al–Ni shape memory alloy. *Materials characterization*, 2008, Vol. 59, no. 7, p. 920-929. ISSN 10445803.

[16] WEI, Z. G., et al. Reverse transformations in Cu-Al-Ni-Mn-Ti alloy at elevated temperatures. *Acta materialia*, 1996, Vol. 44, no. 3, p. 1189-1199. ISSN 13596454.

[17] MORRIS, M. A., LIPE, T. Microstructural influence of Mn additions on thermoelastic and pseudoelastic properties of Cu-Al-Ni alloys. *Acta metallurgica et materialia*, 1994, Vol. 42, no. 5, p. 1583-1594. ISSN 09567151.

[18] BENJAMIN, J. S. Mechanical alloying-A perspective. *Metal Powder Report*, 1990, Vol. 45, no. 2, p. 122-127. ISSN 00260657.

[19] SURYANARAYANA, Ch. Mechanical alloying and milling. *Progress in materials science*, 2001, Vol. 46, no. 1, p. 1-184. ISSN 00796425.

[20] SONI, P. R. Mechanical alloying: fundamentals and applications. *Cambridge Int Science Publishing*, 1998. ISBN 9781898326564.

[21] SURYANARAYANA, C., IVANOV, E., BOLDYREV, V. V. The science and technology of mechanical alloying. *Materials Science and Engineering: A*, 2001, Vol. 304, p. 151-158. ISSN 09215093.

[22] COURTNEY, T. H. Modeling of mechanical milling and mechanical alloying. *Reviews in Particulate Materials*, 1994, Vol. 2, p. 63-116.

[23] PIŇOS, J. Studium vlastností kovových materiálů připravených technologií nízkoteplotního kinetického naprašování Brno: Vysoké učení technické v Brně, Fakulta strojního inženýrství, 2013. 92 s. Vedoucí diplomové práce: Ing. Jan Čížek, Ph.D.

6. List of symbols and abbreviations

A_f	austenite finish temperature
A_s	austenite start temperature
M_f	martensite finish temperature
M_s	martensite start temperature
LM	light microscopy
MA	mechanical alloying
PE	pseudoelasticity
PM	powder metallurgy
EDX	energy dispersive X-ray spectroscopy
HIP	hot isostatic press
RPM	revolutions per minute
SEM	scanning electron microscopy
SMA	shape memory alloys
SME	shape memory effect
XRD	X-ray diffraction
OWSMA	one-way shape memory alloys
OWSME	one-way shape memory effect
TWSMA	two-way shape memory alloys
TWSME	two-way shape memory effect

A. EDS mapping of elemental powders

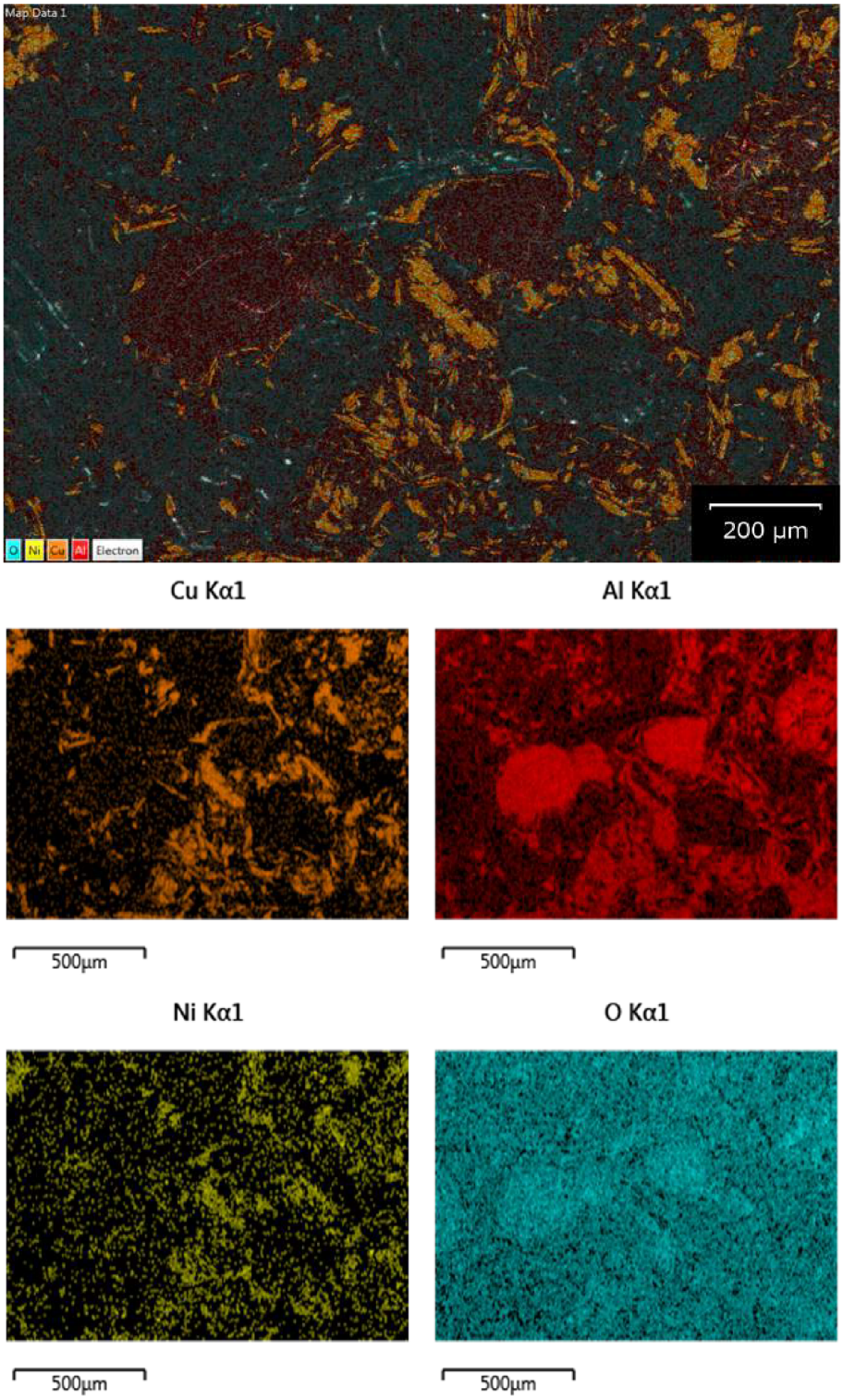

Figure A.1: EDS mapping of elements in powders P01.

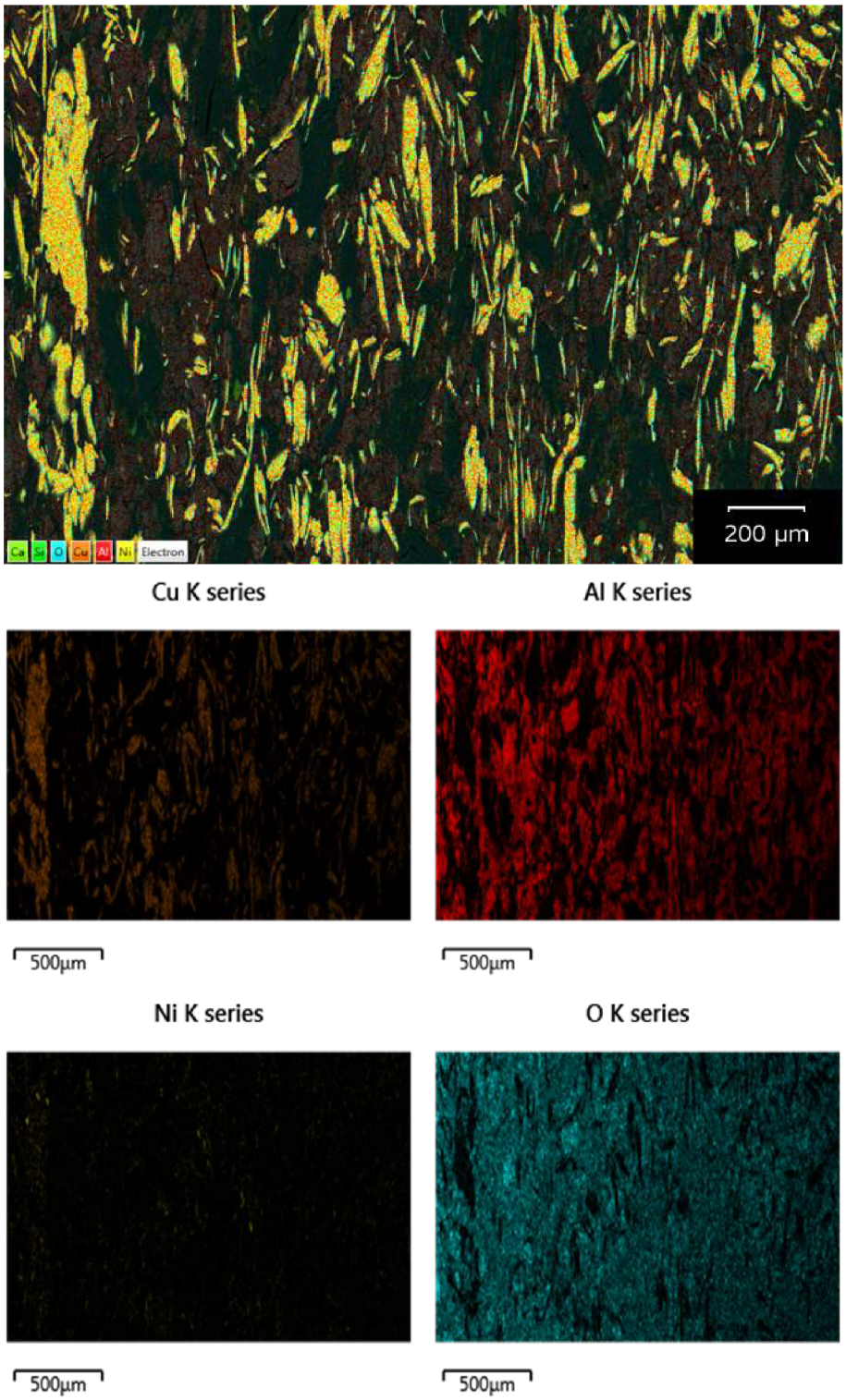

Figure A.2: EDS mapping of elements in powders P02.

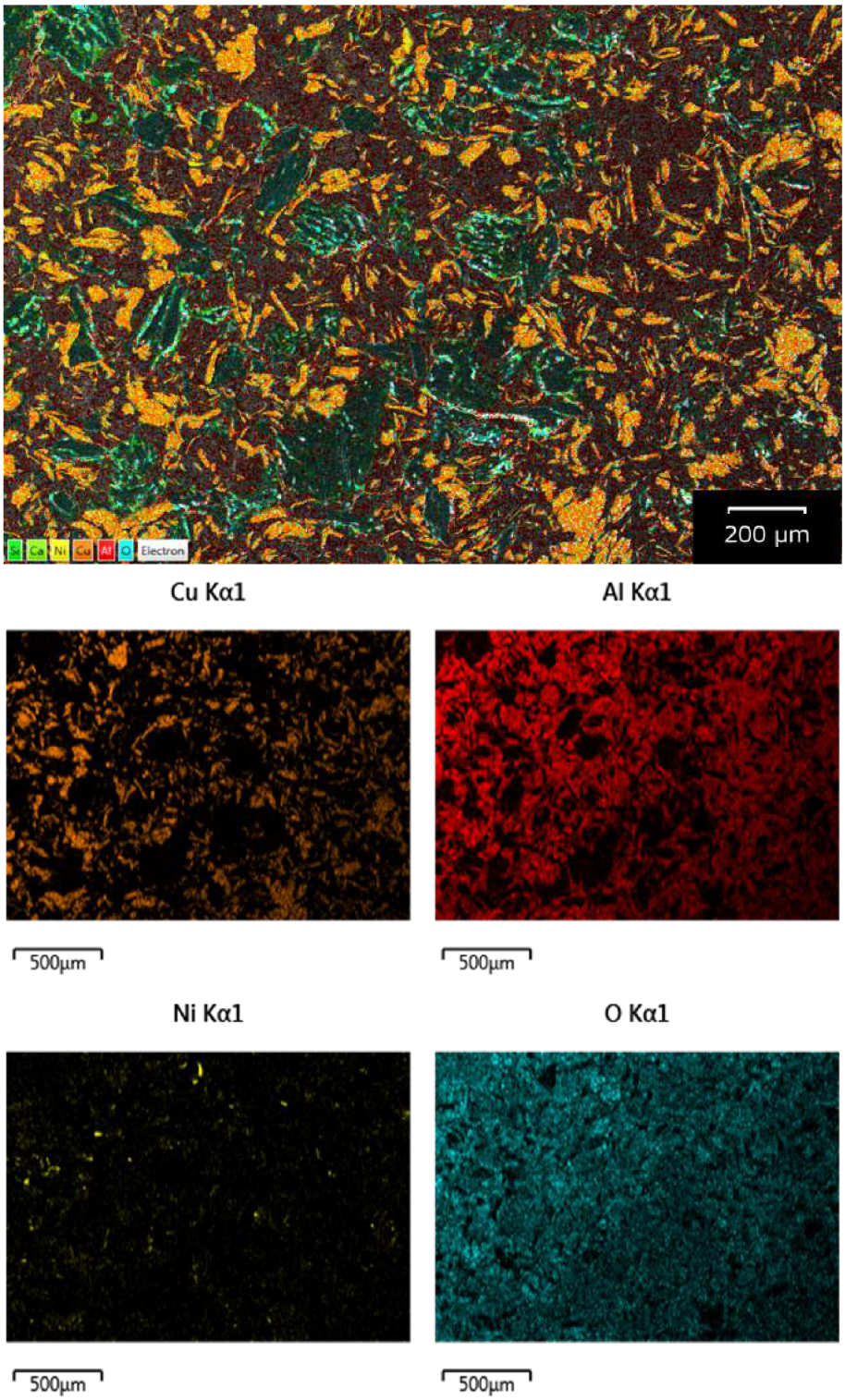

Figure A.3: EDS mapping of elements in powders P03.

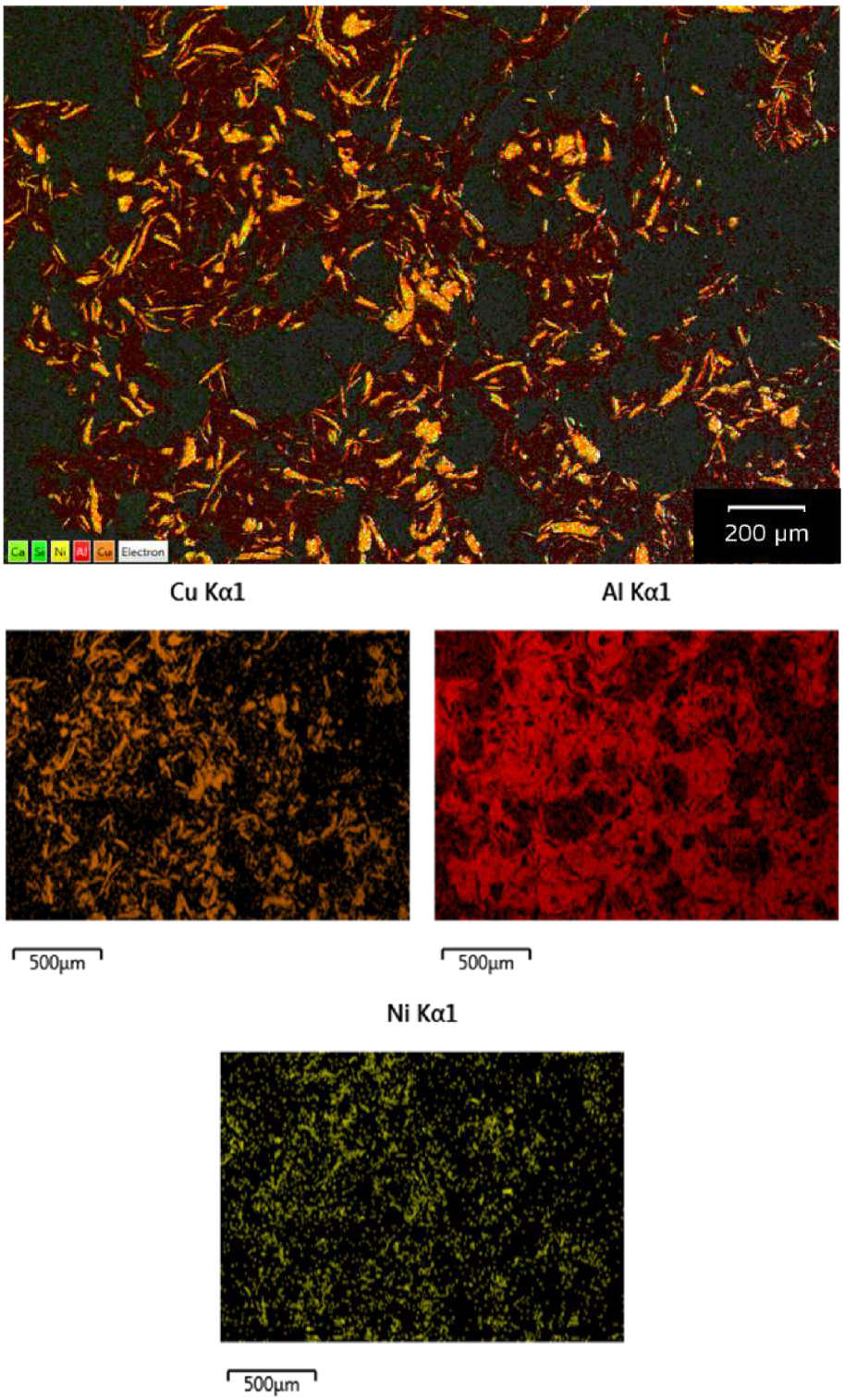

Figure A.4: EDS mapping of elements in powders P04.

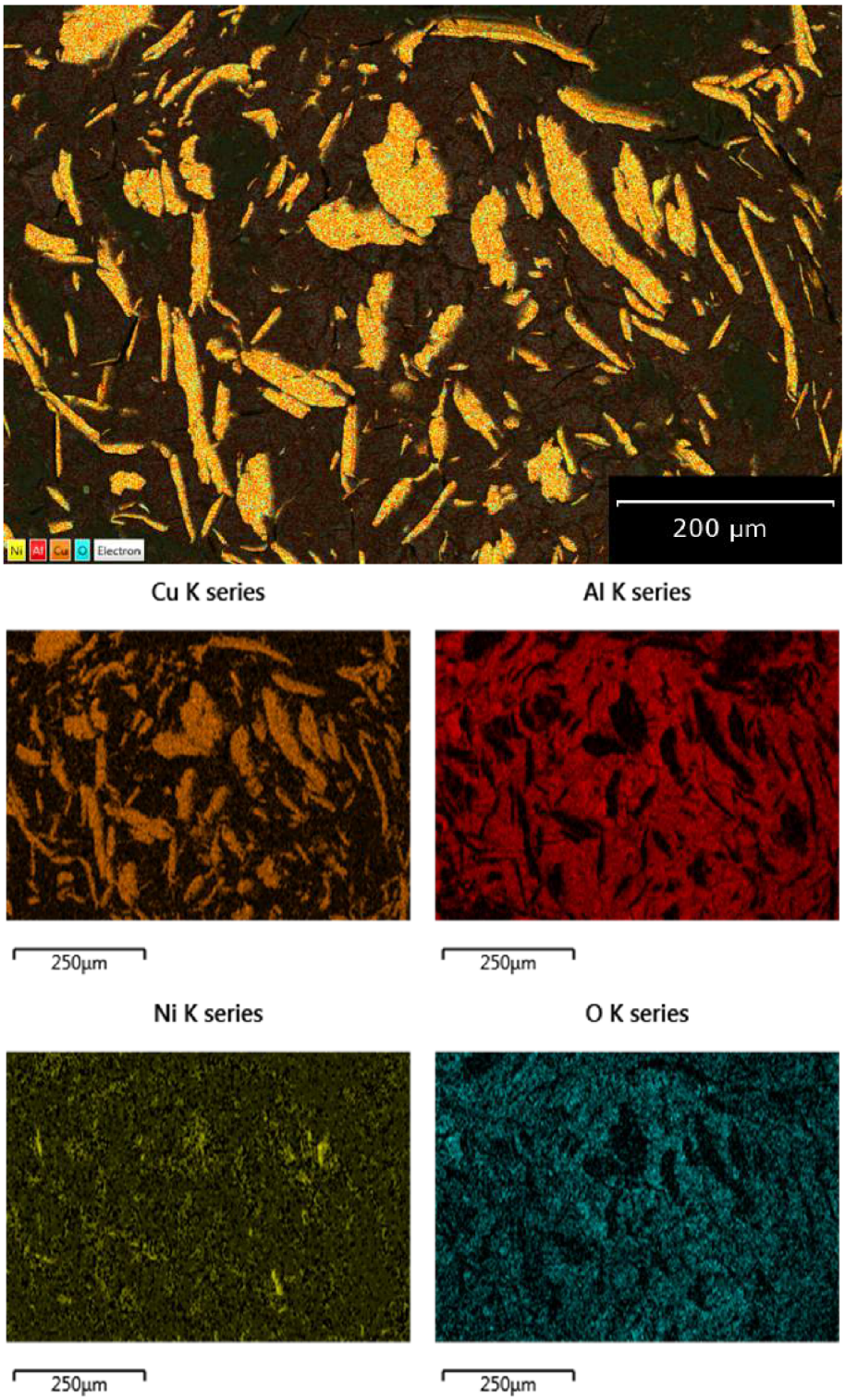

Figure A.5: EDS mapping of elements in powders P05.

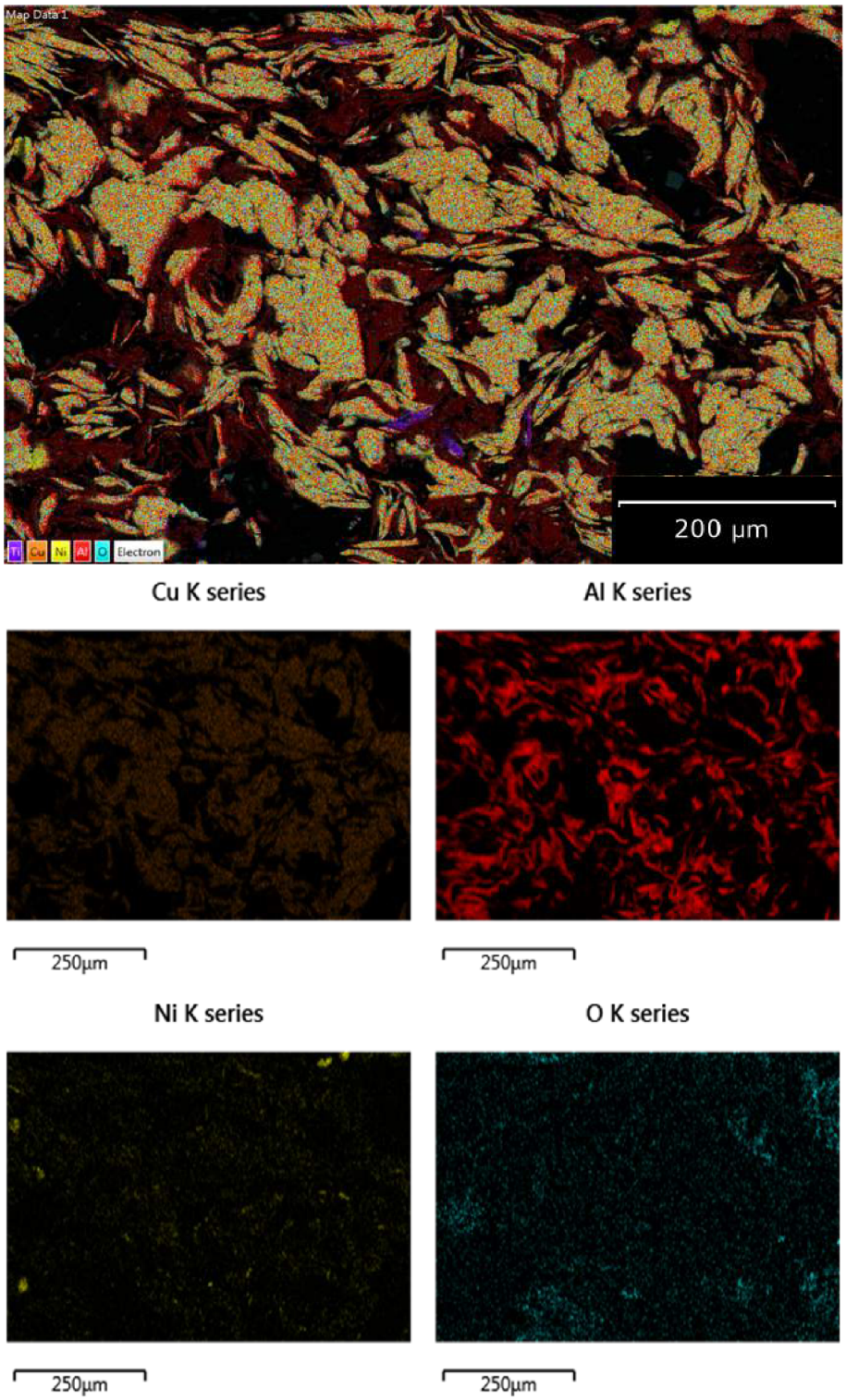

Figure A.6: EDS mapping of elements in powders P06.

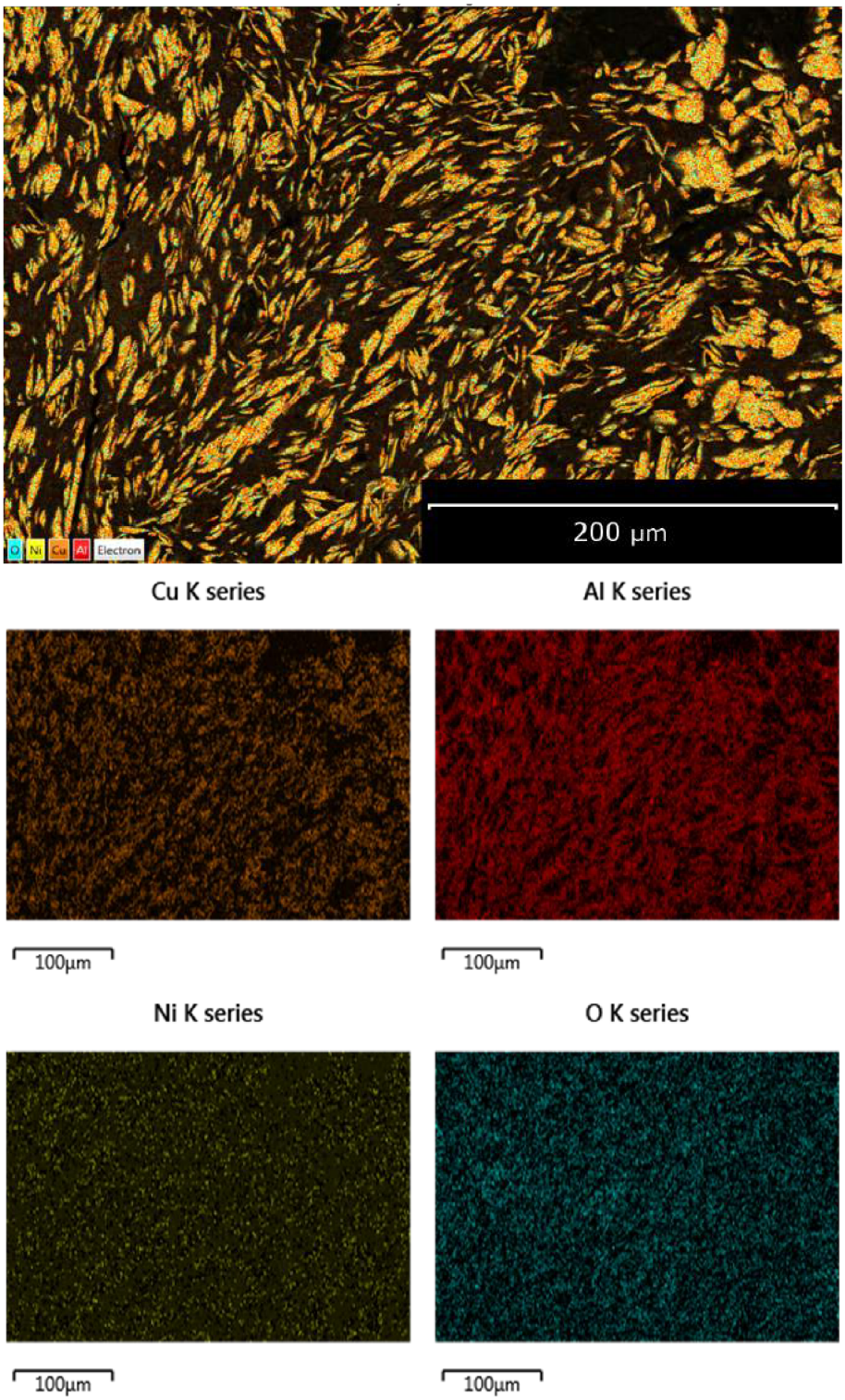

Figure A.7: EDS mapping of elements in powders P07.